Schweizerische Eidgenossenschaft
Confédération suisse
Confederazione Svizzera
Confederaziun svizra

Department of the Environment,
Transport, Energy and Communication DETEC

Swiss Federal Office of Energy SFOE
Energy Research

Final report

PASSCO

Passivating contacts for high-efficiency crystalline silicon solar cells

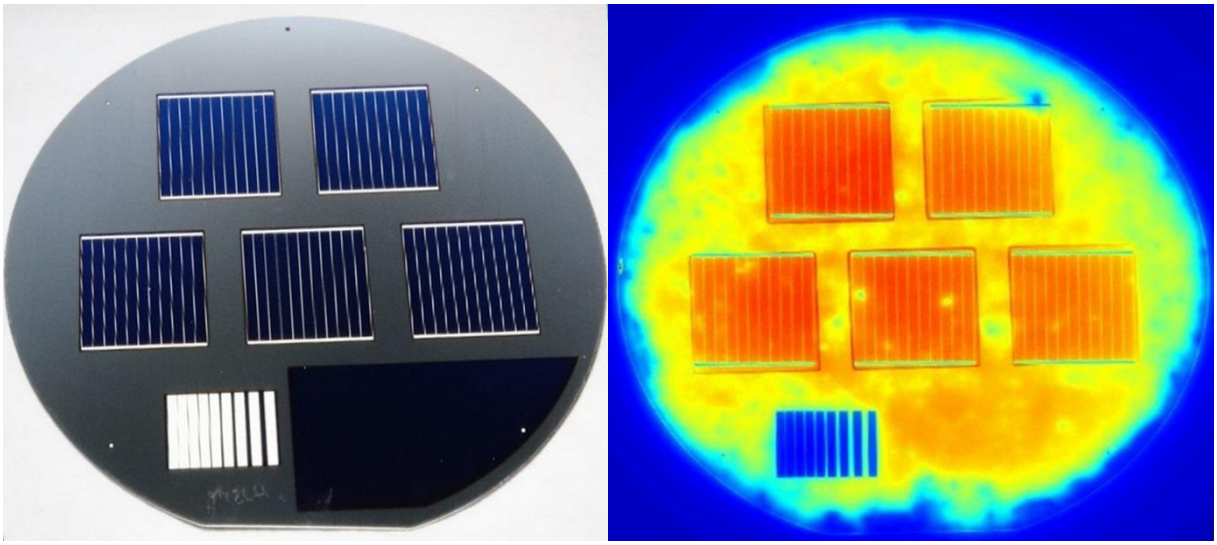

Date: 28 February 2018

Place: Bern

Publisher:
Swiss Federal Office of Energy SFOE
Research Programme XY
CH-3003 Bern
www.bfe.admin.ch
energieforschung@bfe.admin.ch

Agent:
Ecole Polytechnique Fédérale de Lausanne (EPFL)
Photovoltaics and Thin Film Electronics Laboratory (PV-Lab)
Maladière 71b
CH-2000 Neuchâtel

Author:
Franz-Josef Haug, EPFL PV-Lab, franz-josef.haug@epfl.ch
Andrea Ingenito, EPFL PV-Lab, andrea.ingenito@epfl.ch
Christophe Ballif, EPFL PV-Lab, christophe.ballif@epfl.ch
pvlab.epfl.ch

SFOE head of domain: Stefan Oberholzer, stefan.oberholzer@bfe.admin.ch
SFOE programme manager: Stefan Nowak, stefan.nowak@netenergy.ch
SFOE contract number: SI/501253-01

Summary

Crystalline silicon solar cells are the most widely used photovoltaic technology, but there is still a large margin of improvement. Compared to record devices, most cells in mainstream production have low open circuit voltage because generally they do not use passivating contacts. A new type of passivating contact could resolve this issue. It uses a passivation layer of silicon oxide that is compatible with high processing temperatures, and the oxide is thin enough for tunnelling transport into an adjacent layer of highly doped polycrystalline silicon. Remaining hurdles are that most of the reported work applied to electron-contacts for n-type silicon, and that complicated manufacturing techniques were used to demonstrate high efficiency solar cells. In the PASSCO project, we investigated passivating contacts to the more commonly used p-type silicon, and we used plasma deposition in a parallel plate reactor, an industrially compatible technique. We developed passivating hole contacts to mitigate the low to medium passivation quality of rear-contacts in current standard solar cells, and we demonstrated passivating electron contacts for the junction at the front-side.

The experimental work was focused on the fabrication of the doped layers on top of the interfacial tunnel-oxide and on the subsequent formation of the passivating contact by annealing. The processing with plasma deposition offers several advantages such as single-side processing of the deposited layers, excellent adhesion, tailored doping concentrations, and full control of bandgap and nano-structure. On this basis we were able to develop passivating contacts that comply with the thermal budgets used for emitter diffusion and for the rapid thermal annealing of contact metallization. In purpose-built demonstration devices, these contacts achieved open circuit voltages above 700 mV and fill factors higher than 80% (up to 84% in planar devices) with efficiencies up to 22.6%. Finally, we also succeeded in integrating our passivating rear contacts into the firing process of industrial cells, resulting in a very promising efficiency of 21.4%. The PASSCO project thus contributes several new building blocks that allow solar cell manufacturers an upgrade of their production lines and to exploit the advantages of passivating contacts. This should ultimately transform into modules with higher performance and higher energy yield, allowing lower cost of solar electricity.

Zusammenfassung

Kristalline Silicium-Solarzellen sind die am weitesten verbreitete PV-Technologie, aber es gibt immer noch grosses Potential für Verbesserungen. Zum Beispiel haben Zellen aus der industriellen Produktion geringere Leerlaufspannungen als Rekordzellen, da sie in der Regel keine passivierenden Kontakte haben. Ein neuartiger passivierender Kontakt könnte dieses Problem lösen. Er besteht aus einer Passivierungsschicht aus Silicium-Oxid, die hohe Prozesstemperaturen aushält, gleichzeitig ist die Oxidschicht dünn genug, um Tunneltransport in eine darüber liegende Kontaktschicht aus hoch-dotiertem, polykristallinem Silicium zu gewährleisten. Es verbleiben die Hürden, dass die meisten dieser passivierenden Kontakte für n-dotierte Wafer entwickelt wurden, und dass komplizierte Verfahren benutzt wurden, um Rekordzellen herzustellen. Im PASSCO-Projekt untersuchten wir passivierende Kontakte für p-dotierte Wafer, die weiter verbreitet sind, und wir verwendeten Plasma-unterstützte Gasphasenabscheidung in einem Reaktor mit parallelen Elektroden, eine industriell einsetzbare Technologie. Wir entwickelten passivierende Löcher-Kontakte um die schlechte Passivierung der Rückkontakte in Standardzellen zu verbessern, und wir konnten passivierende Elektronen-Kontakte für den p-n Übergang an der Vorderseite herstellen.

Die experimentellen Arbeiten fokussierten auf die Herstellung der dotierten Schichten auf dem Tunneloxid und auf die anschliessende Ausbildung der passivierenden Kontakte in einem Temperschritt. Plasmaabscheidung bietet dabei mehrere Vorteile, zum Beispiel einseitige Abscheidung, ausgezeichnete Haftung, massgeschneiderte Dotierung, sowie eine vollständige

Kontrolle über die Bandlücke und die Nanostruktur. Dies versetzte uns in die Lage, passivierende Kontakte zu entwickeln, die mit den Temperaturprofilen der Phosphordiffusion und des Feuerschrittes der Metallisierung kompatibel sind. In speziellen Testzellen lieferten diese passivierenden Kontakte Leerlaufspannungen von mehr als 700 mV und Füllfaktoren von mehr als 80% (84% im Falle einer planaren Zelle), dem entsprechen Wirkungsgrade von bis 22.6%. Ausserdem konnten wir einen passivierenden Kontakt in den Feuerprozess einer industriellen Solarzelle integrieren, die damit einen sehr vielversprechenden Wirkungsgrad von 21.4% erzielte. Das PASSCO Projekt zeigt damit verschiedene Prozesssequenzen auf, mit denen Hersteller ihre Produktionsstrassen aufrüsten und die Vorteile von passivierenden Kontakten nutzen können. Dies ermöglicht effizientere Module mit besserer Energieausbeute und Solarenergie zu niedrigeren Kosten.

Résumée

Les cellules solaires en silicium cristallin constituent la technologie photovoltaïque la plus utilisée au niveau mondial. Malgré cela, une marge d'amélioration importante subsiste encore. En comparant les cellules records et les cellules standards produites actuellement par l'industrie, les tensions de circuit ouvert des cellules industrielles sont basses car elles n'utilisent pas de contacts dit passivants. Une nouvelle génération de contacts passivants peut permettre de surmonter cette limitation. Ceux-ci sont constitués d'une couche d'oxyde de silicium pouvant supporter des processus « standards » à haute température et aussi suffisamment fines pour permettre le tunneling des porteurs de charge jusque dans une couche de contact adjacente en silicium polycrystallin fortement dopé. Ces contacts passivants ont été démontrées principalement dans le cas des plaquettes de type n. De plus, la réalisation de cellules à très haut rendement nécessite de nombreuses et complexes étapes de fabrication difficilement industrialisable. Dans le projet PASSCO, nous avons d'une part étudié des contacts pour les plaquettes de type p car plus utilisées dans l'industrie, et d'autre-part, nous avons utilisé la technologie de dépôt par plasma dans un réacteurs à électrode parallèle qui est également une technologie compatible avec les processus de fabrication industrielle. Nous avons développé des contacts passivants de type p dans le but d'améliorer la qualité de passivation des contacts arrières et ainsi pouvoir remplacer les contacts des cellules standards actuelles. Nous avons également développé, dans le cadre du projet, des contacts de type n pour la jonction en face avant de la cellule.

Les travaux se sont focalisés sur les procédés de fabrication des couches dopées, sur l'oxyde de silicium à l'interface et sur la formation du contact passivant pendant le recuit à haute température. Le dépôt par plasma offre plusieurs avantages, p.ex. le dépôt sur un seul côté, une bonne adhésion, un dopage sélectif, ainsi que le contrôle de la bande interdite et de la structure du contact à une échelle nanométrique. Grâce à cela nous avons pu développer des contacts passivants compatibles avec des procédés déjà utilisé dans l'industrie comme la formation d'un émetteur par diffusion ou les procédés de métallisation par recuit rapide. Pour valider la qualité de nos contacts, nous avons également fabriqué des cellules de démonstration avec lesquelles nous avons obtenu des valeurs de tension en circuit ouvert supérieure à700 mV, des facteurs de forme supérieur à 80% (même 84% avec une cellule plate), et des efficacités allant jusqu'à 22.6%, avec les deux faces passivées. Finalement, l'intégration de couches différentes avec le recuit rapide d'une cellule industrielle a atteint une efficacité très prometteuse de 21.4%. Le projet PASSCO offre donc plusieurs nouveaux blocs technologiques permettant aux producteurs industriels d'améliorer leur procédé et de viser le développement de cellules solaire de nouvelle génération. A terme, cela permettra une augmentation de la performance des modules et une réduction des coûts de l'électricité solaire.

Contents

List of abbreviations

a-Si	amorphous silicon
Al-BSF	Aluminium Back Surface Field
ALD	Atomic Layer Deposition
c-Si	crystalline silicon
chem. ox.	Chemical oxide
η	efficiency
ECV	Electrochemical Capacitance-Voltage profiling to determine doping profiles
FF	Fill Factor (subscripts “0” for upper limit and “s” to include series resistance)
FE	Field Emission (used to describe charge-carrier tunnelling)
FZ	floating zone (crystalline silicon of highest material quality)
FGA	Forming Gas Anneal (usually 20 to 40 min at 450°C in nitrogen with 5% hydrogen)
ISE	Institut für Solare Energiesysteme, an institute of the German Fraunhofer Society
ISFH	Institute für Solarenergieforschung, an institute affiliated to the University of Hannover
ITO	Indium-Tin-Oxide, a transparent contact material
iVoc	implied open circuit voltage (implied by the saturation current, not measured in a cell)
j_0	saturation current density
j_{sc}	short circuit current density
µc-Si	microcrystalline silicon
µs	micro-second
ms	milli-second
MPP	Maximum Power Point
nm	nano-meter
pFF	pseudo-FF (measured by SunsVoc without series resistance)
PE-CVD	Plasma Enhanced Chemical Vapour Deposition
PERC	Passivated Emitter and Rear Cell
POLO	Poly-Silicon on Oxide
ρ_c	contact resistivity
SiCx	silicon carbide, here with low carbon content between 3 and 5%
SIMS	Secondary Ion Mass Spectroscopy
SiNx	silicon nitride, here usually with low nitrogen content, used as hydrogen source
SiOx	silicon oxide, here usually grown phase separated as silicon crystallites in SiOx matrix
SunsVoc	measurement of the Voc at varying illumination level without current flow
τ_{eff}	effective lifetime
TEM	Transmission Electron Microscopy
TE	Thermionic Emission (transport by thermal activation over a Schottky barrier)
TFE	Thermionic Field Emission (tunnelling assisted transport over/through a Schottky barrier)
TLM	Transfer Length Method (to determine sheet- and contact-resistance)
TOPCon	Tunnel Oxide Passivating Contact
V_{oc}	open circuit voltage
v_s	surface recombination velocity

1 Introduction

Since their first application for early satellites in space, solar cells have become a terrestrial energy source with widespread application. Over these 40 years, the cost of solar modules decreased by more than 20% for every doubling of the module production [1]. As a result, photovoltaic electricity provides today about 1.3% of the global electricity-needs, and it is forecasted to take a leading role in our future CO_2-free energy mix. Among the different photovoltaic technologies, crystalline silicon (c-Si) always had a leading position because it is a benign and abundant material, because its processing is well-known from the micro-electronics industry, and because it can be integrated in solar modules with extraordinary lifetime. Reducing further the cost of solar electricity requires continuous efforts in research to further increase the efficiency, and in development to apply the latest findings towards cost-effective manufacturing.

2 Context

2.1 Background / State of the art

About 80% of all silicon cells are currently manufactured with a standard process that uses phosphorous diffusion for the front junction, and a rear-contact with **aluminium back surface field** (Al-BSF) as illustrated in in the upper panel of Figure 1. Countless improvements over the last two decades made it possible to integrate this process into a very lean sequence, but the resulting cells have only moderate open circuit voltage (Voc) due to recombination of electrons at the rear contact where silicon is in direct contact with the aluminium metallization. In manufacturing there is currently a trend towards **passivated emitter and rear cells** (PERC). In this cell type, the rear surface is covered by a passivating layer of Al_2O_3 with small openings for the contacts. Thus, recombination losses are reduced since the area in contact with the metal is smaller, but the series resistance is increased due to the reduced contact area. This leads to trade-off between Voc and FF.

A comparison of the upper two panels in Figure 1 illustrates that the PERC design uses the same wafer type and the same front contact as the standard cell with the Al-BSF. The difference lies in the fabrication of the rear contact which adds two steps to the manufacturing sequence; one for the deposition of the passivating Al_2O_3 film and a second for the opening of the contact areas. After that, the aluminium-metallization is screen-printed and fired together with the silver-metallization at the front. This contact strategy was first demonstrated in 1989 with a passivation layer of SiO_2 and openings defined by photolithography [2]. Industry was reluctant to adopt the concept and instead ramped up the BSF process with low-cost, p-type multicrystalline wafers. Industrialization of PERC-concepts had to wait for the development of atomic layer deposition (ALD) to replace the SiO_2 rear passivating layer by Al_2O_3, laser-opening of the passivation with high throughput, and tailored aluminium screen-printing pastes [3, 4]. With these ingredients, the PERC concept became a viable option for industry, and it is currently applied to ca. 20% of all silicon solar cells. Forecasts predict that it will replace the BSF concept within the coming 10 years [1]. Thus, the limitation of the open circuit voltage may be improved from typically 640 mV to 680 mV, but typical PERC cells are still short of the Voc values far above 720 mV that have been demonstrated with a passivating contacts in the current world-record devices. This suggests that the Voc will ultimately remain a limiting factor for PERC technology.

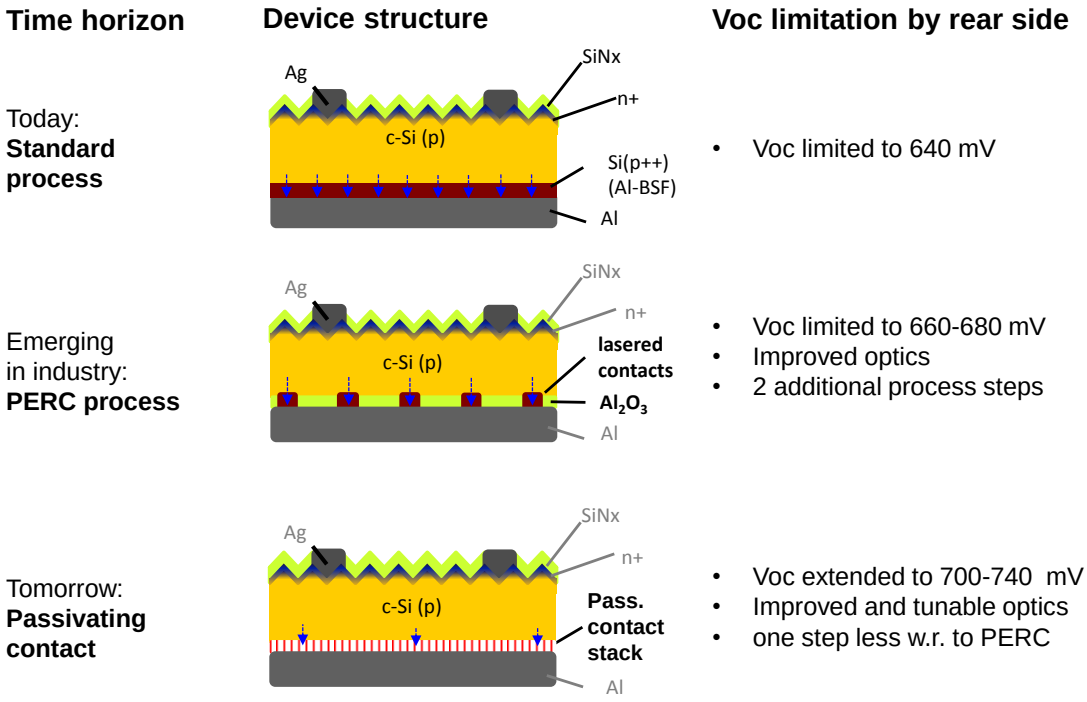

Figure 1: Transition from today's BSF standard cell with its limitation by recombination at the full area rear metallization (blue arrows, top panel) to an improved design with smaller contact area through local openings (middle panel). The strategy of passivating contacts avoids, or at least minimizes, the direct contact to the metal (lower panel).

Taking up earlier work on solar cells with SiO_2 tunnelling layers [5], researchers of the Fraunhofer Institute for Solar Energy-Research (ISE) proposed a different concept which is based on a **tunnel-oxide passivating contact** (TOPCon). They were able to demonstrate an efficiency of 25.7% [6] which is the current world record for both-side contacted silicon solar cells. The deposition of the passivating layer involves only one additional step and there is no need for laser opening. However, the TOPCon devices of ISE are usually based on n-type contact layers that apply to n-type wafers in combination with a boron-diffused junction at the front. The industrialization of this technology would require major changes to standard manufacturing processes.

2.2 Motivation of the project

The PASSCO project intended to select the best of the different contacting procedures outlined above, and to combine them into a new solar cell design. The intention is to benefit from the well-developed n-type front contact and to add a passivating contact to the full rear area. The implementation of such a process should be an upgrade to established standard processes rather than a disruptive change.

In order to remain compatible with key ingredients of standard cell processing, there are three requirements:

- Work on p-type wafers since they are more easily available and less costly than n-type wafers.
- Keep the diffused front junction which is an established procedure and a necessary step for improving wafers of medium quality by gettering.
- Remain compatible with the thermal budget encountered during the processing steps of standard cells, either the diffusion of the front-contact or the firing of the metallization.

2.3 Goals

The main goal of the PASSCO project was the development of p-type passivating contacts that apply to the full rear surface. Thus, recombination losses of the BSF contact can be avoided, and local contact openings are not needed. A secondary goal of the PASSCO project applied to the medium- or long term and consisted of an n-type passivating front contact that forms the p-n junction at the front. This strategy intends to offer to cell-manufacturers the building blocks that are needed to incrementally upgrade their process chain with small steps rather than requiring them to implement novel and disruptive concepts.

3 Approach and methodology

At the time of writing the proposal in 2014, the main approach towards passivating contacts was the heterojunction solar cell. Since it uses passivation and contact layers of amorphous silicon, all subsequent processing steps are limited to ca. 200°C. The silver particles in the metallization pastes cannot sinter well at such temperatures, resulting in resistivities that are much higher than those of high-temperature pastes. Plated contacts are a possible alternative to overcome this limitation. Plating typically needs a seed layer of nickel-silicide, but the silicide forms only between 300 and 400°C. Consequently, a large amount of work was initially foreseen in WP2 to develop heterojunction solar cells that tolerate temperatures up to 400°C.

Passivating contacts based on tunnel oxides were investigated in the 80ies and early 90ies [5], but then they were either abandoned in favour of PERC and PERL cells which are based on the conceptually simpler pn-junctions, or development was continued in companies without being published in the literature. However, tunnel oxides had an impressive come-back in 2014 in a series of articles published by the Fraunhofer Institute for Solar Energy Systems [7–10]. Annealed tunnel oxide passivating contacts were thus included as research topic in WP3 of the proposal and fireable ones as more exploratory work in WP4.

During the first year of the PASSCO project in 2015, it emerged that industries are rather reluctant to take up plated metallization processes. At the same time, passivating contacts were embraced more enthusiastically, first because they promise easier integration into standard manufacturing processes on short term (c.f. Figure 1), and second because they are also a feasible option on a timeframe “beyond PERC”.

Consequently, the work on heterojunctions was focussed on p-type microcrystalline layers in order to improve optical performance and contact resistivity (c.f. section 4.2). Work foreseen for extending the temperature tolerance was rescheduled to assist the activities on tunnel-oxide passivating contacts (c.f. sections 4.3.1 and 4.3.2).

4 Results

The following subsections discuss the progress in the different work-packages of the PASSCO project, starting from the development of passivating layers made of SiOx in WP1, and a discussion of the limitations by due to contact resistance in heterojunction cells with amorphous passivation layers in WP2. After that, the development of high-temperature stable passivating contacts is discussed in two subsections; WP3 presents the progress with processes that employ long annealing, WP4 covers processes with rapid firing. Finally, WP5 gives a short outlook on the reliability of annealed contacts with respect to extended UV-illumination

4.1 SiOx passivation layers (WP1)

Passivating tunnel contacts rely on a very thin insulating film that passivates the silicon surface and separates the wafer from the contact material. The simplest tunnelling layer is a thin film of silicon oxide, in most cases deposited by annealing in oxidizing atmosphere. The goals of this WP were defined two-fold. The first was the development of thermal oxidation and hydrogenation of the thermal oxide layers by combining newly installed infrastructure and existing tools at PV-Lab. The second goal was the development of a wet-chemical oxidation process since this can be integrated more easily into a manufacturing sequence where wet-chemistry is necessarily employed for wafer cleaning and texture etching.

Passivation and recombination phenomena in crystalline silicon are most easily assessed in terms of the minority carrier lifetime which is accessible by a simple and contact-free measurement. Figure 2 shows the highest reported values of the bulk lifetime of p-type floating zone (FZ) wafers passivated with thermally grown SiO_2 after hydrogenation [6],[11] or with Al_2O_3 [9]. Since these methods provide virtually perfect passivation, the resulting lifetimes can be associated with the bulk of the wafers. For resistivities between 1 and 5 Ωcm as used in this project, the bulk lifetimes vary between 2 and 8 ms.

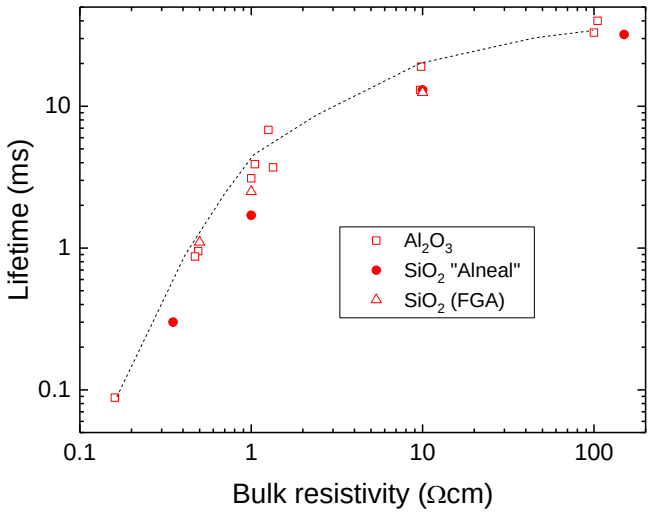

Figure 2: Dependence of the bulk lifetime in p-type FZ wafers on the wafer resistivity [8, 9, 20]. Open squares denote passivation with Al_2O_3, circles and triangles represent passivation layers of SiO_2 combined with different types of hydrogenation.

When the quality of the surface passivation is not ideal, lower lifetimes can be associated to recombination losses at the surface, and for this reason they are called **effective lifetimes**. On this basis, two main goals were defined for WP 1. The first was the definition of a process for passivation with thermal oxide. Since the passivation with thermal oxides and the impact of hydrogenation on this type of oxide is well understood, it was used to qualify the development of a hydrogenation process with respect to a known reference. Thus, WP1 aimed at demonstrating effective lifetimes > 1 ms for FZ wafers with resistivities between 1 and 5 Ωcm. Note that this is also a minimum requirement for open circuit voltages above 700 mV in silicon solar cells.

The second goal was the development of tunnelling layers by a wet-chemical oxidation process since this can be integrated easily into the standard cleaning sequence. It has the additional advantage of being self-saturating in the desired thickness range of tunnelling layers which is between 1.2 and 1.5 nm [12]. Thermal oxides may potentially provide better passivation, but they would require an

additional manufacturing step in a furnace, and for thin layers it is more challenging to control the thickness precisely.

The black bars in Figure 3 represent effective lifetimes measured on thermally oxidized n-type FZ wafers during a subsequent hydrogenation treatment. We used oxidation for 5 min at 900°C which yields an oxide thickness between 13 and 14 nm on both sides. Directly after deposition, the thermal oxide provides only very poor passivation as evidenced by the effective lifetime of 500 µs. In order to improve the passivation, hydrogenation from a SiNx layer was applied. Since the SiNx-layer is deposited by PE-CVD from silane (SiH_4) and ammonia (NH_3), it contains several atomic percent of hydrogen. Depending on the deposition temperature and the stoichiometry of the layer, hydrogen is released from SiNx at temperatures between 400 and 600°C. The growth of the SiNx-layer does not appreciably increase the effective lifetime, but a large improvement is observed after an annealing for 30 min on a hot-plate at 450°C because a part of the released hydrogen diffuses towards the underlying wafer where it passivates interface states between silicon and silicon oxide. Since SiNx can provide field effect passivation to n-type material due to its resident positive charge, the true improvement of the thermal oxide can only be assessed after removing the SiNx layer selectively in phosphoric acid. Finally, the effective lifetime of the sample achieved a lifetime of 1.75 ms. Thus it fulfils the first objective of the WP and demonstrates the viability of hydrogenation.

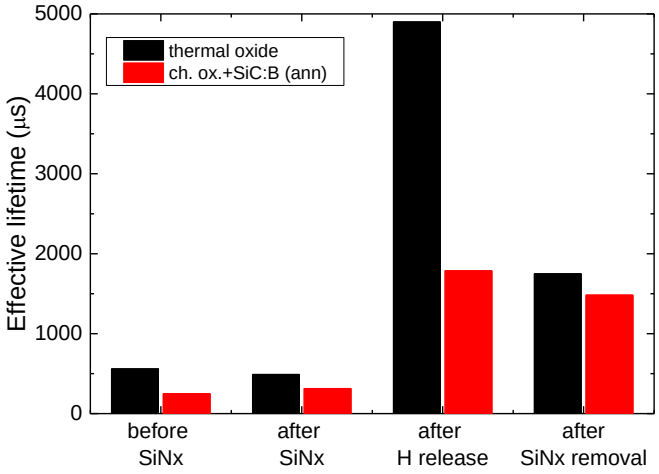

Figure 3: Effective lifetimes during a typical development cycle measured on symmetric test structures. Black bars denote a thermal oxide reference from an early stage of the development. The red bars represent a complete passivating contact structure; after the last step this sample is ready for testing the contact resistivity or for use in a solar cell.

Once the hydrogenation process was successfully developed and proven for the thermal reference oxide, it was applied to the more relevant case of complete contact structures that consist of a thin oxide layer for passivation and of a doped layer for contacting. The interfacial oxide was grown wet-chemically in hot nitric acid after the standard wafer-cleaning and -etching procedure. By themselves, chemical oxides provide only very poor passivation [13], but they were reported to yield excellent tunnelling contacts in combination with an n-type layer after annealing and hydrogenation [14]. In our case, the doped layer consists of an amorphous layer of boron-doped silicon-carbide. It is intended to provide electric contact to the external metallization and to serve as reservoir for diffusion of dopants through the oxide into the wafer. It contains a small amount of carbon which promotes adhesion to the underlying oxide and bonds more strongly to hydrogen than silicon.

In the early stage of development, both sides of the wafer were treated identically which makes it simpler to relate the effective lifetime to the properties of the surface. The development proceeded by

varying the interfacial oxide, i.e. composition and temperature of the oxidation bath and the residence time of the wafer, the deposition conditions of the doped layer, i.e. plasma power, gas flow and pressure., and the design of the deposited layer itself, i.e. the use of seed-layers or plasma-treatments and its composition and doping. The red bars in Figure 3 illustrate a typical case, here a 40 nm thick layer of p-type SiCx which has been annealed for 5 minutes at 800°C. Similar to the thermal oxide, there is only a moderate degree of passivation after the deposition, but after hydrogenation an effective lifetime of 1.6 ms is measured. After nitride removal the effective lifetime is only little reduced, suggesting that hydrogenation successfully passivated dangling bonds at the surface of the wafer.

The development cycles underlying to this achievement are discussed on more detail in Section 4.3, notably the thermal budget that the chemical oxide layers can sustain and the impact of doping and annealing conditions on the contact resistance. For processing of solar cells, the contact structure is obviously applied only to one side of the wafer.

Summarizing, three main results were achieved in WP1; first, a process for thermal oxidation was established. Second, reported literature data on the surface passivation of thermal oxides was used as reference to develop a hydrogenation process on the basis of thermal hydrogen release from a SiNx layer. Third, the hydrogenation process was successfully applied to complete contact structures as illustrated in Figure 3.

4.2 Low-temperature heterojunction cells (WP2)

The activities of WP2 started out with efforts to improve the optical properties of heterojunction cells and to obtain better current extraction. An approach to achieve both objectives is to replace the amorphous p-type layer at the front by a more transparent microcrystalline p-type layer. The absorption coefficients shown in the left panel of Figure 4 indicate that this replacement promises a reduction of the parasitic absorption over almost all of the visible spectrum. For infrared wavelengths longer than 750 nm, microcrystalline silicon is expected to absorb more than amorphous silicon; however, on an absolute scale the absorption loss in this spectral region is lower by several orders of magnitude than in the visible part.

Advantages are also expected in terms of current extraction, more specifically because of decreased series resistance; compared to amorphous p-type layers that have contact resistivities in the range of 1.0 to 1.5 Ωcm^2 with the ITO front contact, microcrystalline p-type layers have contact resistivities between 0.45 and 0.5 Ωcm^2 [15]. The right panel of Figure 4 shows that these seemingly minor differences can have a massive impact on FF [16]. For zero contact resistance the so-called **implied FF** (iFF) depends only on the Voc and varies in a narrow band between 83.5 and 84.5%. For a contact resistivity of 1.0 Ωcm^2, the FF_s is reduced to values between 78 and 79% (c.f. eq.(5) of section 9.2). Microcrystalline p-type layers show promise to reach the range between 81 and 82% because of their lower contact resistivities [15].

Based on these theoretical considerations, the actual development of the p-type layer in the front contact is a typical optimization procedure between two opposing trends. On one hand, the layer thickness should be kept as thin as possible since light absorbed in the p-type layer does not contribute to the photocurrent, regardless whether it is amorphous or microcrystalline. On the other hand, if the layer is too thin, it does not contain enough active dopants to build up the electrostatic potential of the p-n junction. In the experiment, wafers with four different thicknesses of amorphous and microcrystalline p-type layer were manufactured. On each of the wafers, five solar cells with an area of 4 cm^2 were defined in the pattern similar to the one shown on the title page. The parameters of the resulting cells are shown in Figure 5.

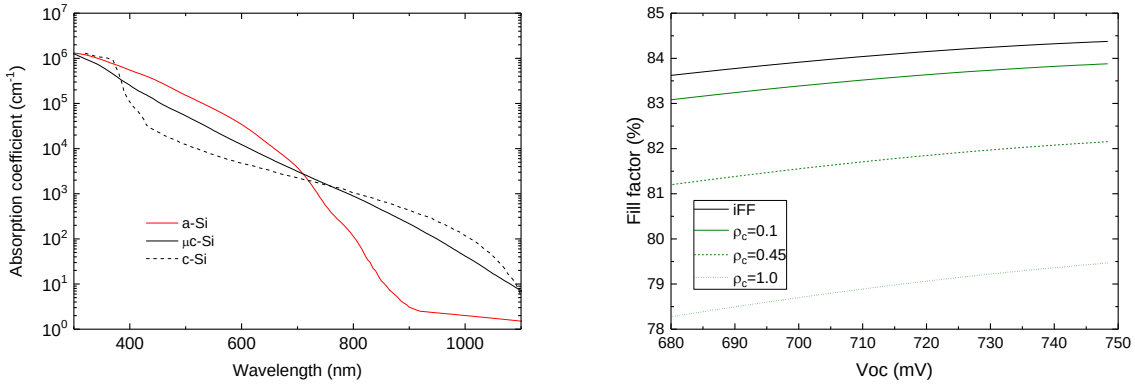

Figure 4: The left panel shows the spectral variation of the absorption coefficients of a-Si (red), µc-Si (black) and c-Si (dashed). The right panel shows the idealized FF for contact resistivity ρ_c of zero (black) and for $\rho_c$values between 0.1 and 1.0 Ωcm^2 (green).

Full symbols in Figure 5 summarize results for amorphous p-type layers. As the thickness of the layer increases from zero (no layer at all) to 6 nm, the upper panels show that the photocurrent decreases whereas the open circuit voltage increases. Multiplying these two parameters with the fill factor reveals an optimum efficiency for a thickness of the p-type amorphous layer of 4 nm.

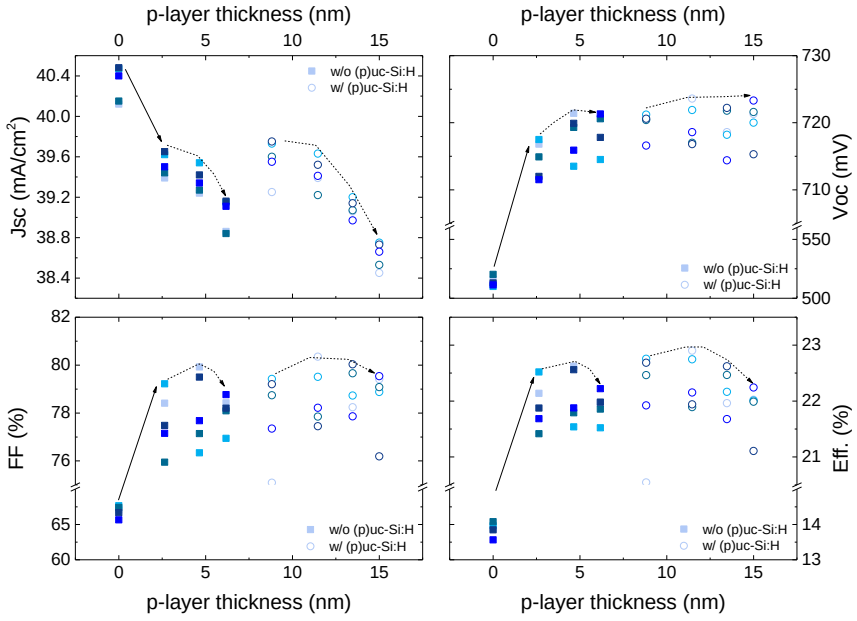

Figure 5: Parameters of heterojunction solar cells with different thicknesses of the p-type layer at the front. Full symbols denote amorphous p-type layers, open symbols represent 2 nm of amorphous layer plus a microcrystalline p-type layer of the shown thickness (nominal values based on deposition time). Arrows are guides to the eye, illustrating the effect of omitting the p-type layer completely (full arrows) and the trends with increasing p-type layer thickness (dashed arrows).

When the amorphous p-type layer (or a part of it) is replaced with a more transparent material such as a microcrystalline p-type layer, the amount of parasitic absorption in the front contact can be reduced. Thus, the corresponding cells represented by open symbols in Figure 5 have slightly higher current density and there is a small, but noticeable gain in open circuit voltage. There is also an improvement in fill factor, but the gain is less expressed than expected on the basis of the contact resistivity.

Overall, a microcrystalline p-type layer with combined thickness of nominally[1] 11 nm results in the best cell, reaching an efficiency of 22.8%.

The experiments show that the FF of heterojunction solar cells is close to a limit because of the doping efficiency of the contact layer. Whereas no further work on this topic was scheduled within the PASSCO project, microcrystalline contact layers are nevertheless implemented successfully in other kind of devices. For example, they are used as tunnel junctions in advanced hybrid perovskite/silicon cells [17]. In these devices the current density is half of the value of single-junction silicon solar cells, the impact of the resistivity is thus much less severe. Another example are cells with interdigitated back contact (IBC). Here, the requirement of transparency is less severe, but the growth kinetics of microcrystalline layers were the key to the demonstration of tunnelling IBCs with a simple masking process [18].

Summarizing WP2, a microcrystalline p-doped layer was developed for the front contact of heterojunctions. It improves the cell performance due to its reduced contact resistivity with the transparent conductive oxide layer, and by a higher transparency compared to purely amorphous layers. A strategic decision was taken to redistribute the efforts that were initially foreseen for increasing the resilience of heterojunction solar cells towards higher processing temperatures. The development of materials initially proposed for this work, i.e. silicon-nitride, –carbide or –oxide, was distributed to other work packages such as WP1 (nitrides) and the high-temperature approaches discussed in the next two sections (WP3 and WP4).

4.3 High temperature passivating contacts (WP3)

This WP is devoted to passivating contacts that resist annealing temperatures between 800 and 900°C for dwell times between minutes and tens of minutes, making use of tasks initially proposed for WP2. Nitride layers turned out to be a versatile hydrogen source for hydrogenation of annealed films. Carbides were found to mitigate the issue of delamination due to their stronger bonding, resisting even firing processes with heating rams up to 50°C/sec. Nanocrystalline oxides were initially tested because of their high transparency which qualified them as candidates for passivating front contacts, later it turned out that their passivation shows extraordinary thermal stabilty.

4.3.1 Annealed p-type SiCx contacts

After the development of the hydrogenation process shown in Figure 3, the development of the passivating p-type contacts continued by testing higher annealing temperatures. It was found that annealing at 900°C results in a complete loss of passivation. This is very different from the case of n-type SiOx passivation layers that were investigated at the same time (c.f. section 4.3.2 unterhalb). In order to understand the loss of passivation, a structural investigation was carried out with transmission electron microscopy (TEM). Figure 6 shows cross-section images and corresponding elemental mappings of the interfacial region in p-type SiCx contact structures.

In the as-deposited state and after annealing at 800°C, Figure 6 shows a well-defined oxide layer in imaging mode as well as in the elemental maps. After annealing at 900°C, the passivating oxide has disappeared from the interface. For this case, further analysis at high resolution reveals that the

[1] The thicknesses of the microcrystalline layers are nominal values based on deposition time. Due to the high hydrogen content in the plasma, microcrystalline silicon grows only after an incubation period. During this time, no material is deposited and an underlying surface may be damaged or even etched by the hydrogen in the plasma. For this reason, the p-type microcrystalline layer was not grown directly on the sensitive passivation layer, but on a 2 nm thick p-type amorphous layer.

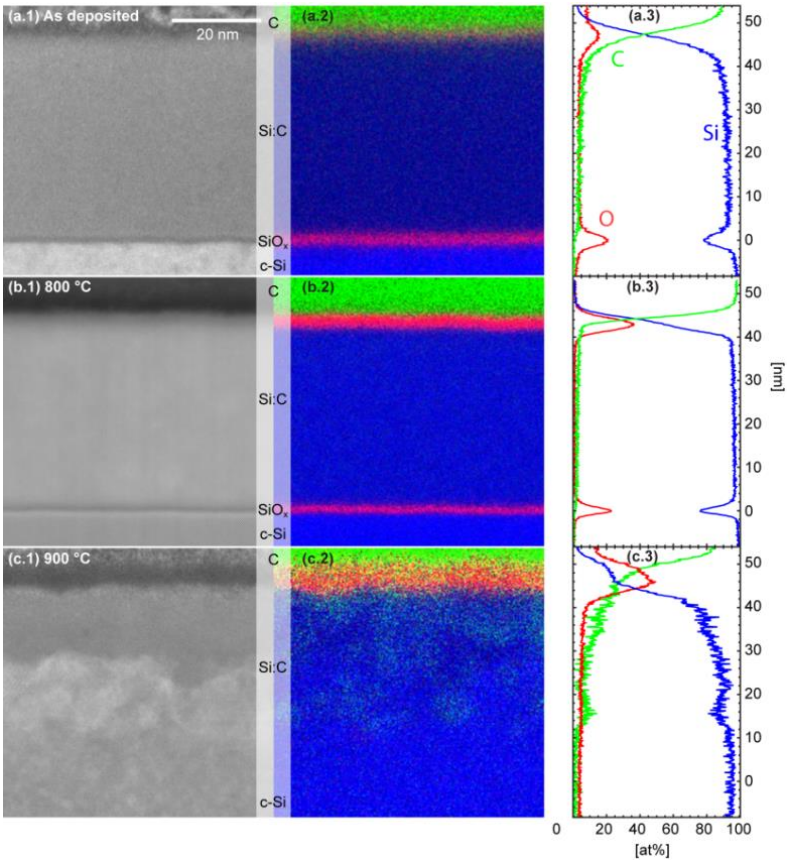

Figure 6: Crystallization of p-type SiCx layer at different temperatures; from top to bottom the images refer to the initial state, and to annealing for 5 min at 800°C and 900°C, respectively. The left panels show TEM cross sections, the middle panels show elemental mappings of the same regions for silicon (blue), oxygen (red) and carbon (green), the right panels show quantified line scans [20].

deposited layer is fully crystallized [19, 20]. It takes up the orientation of the underlying substrate, but it contains many stacking faults and domain boundaries. Since the carbon solubility in silicon is only a few ppm at 900°C, most of it is expelled from the crystallized layer and is collected at the outer interface where it balls up into small grains of stoichiometric silicon-carbide. We tentatively explain the disappearance of the interfacial SiOx layer in Figure 6 by a reaction between loosely bound carbon in the SiCx-layer and oxygen in the interfacial SiOx-layer.

In order to avoid the reaction between carbon and oxygen and to make the passivation of the p-type contact more resilient towards high annealing temperatures, a carbon-free buffer was introduced between the interfacial SiOx layer and the p-type SiCx layer. The TEM analysis in Figure 7 shows that this layer helped to maintain an intact interfacial oxide even after annealing temperatures as high as 925°C.

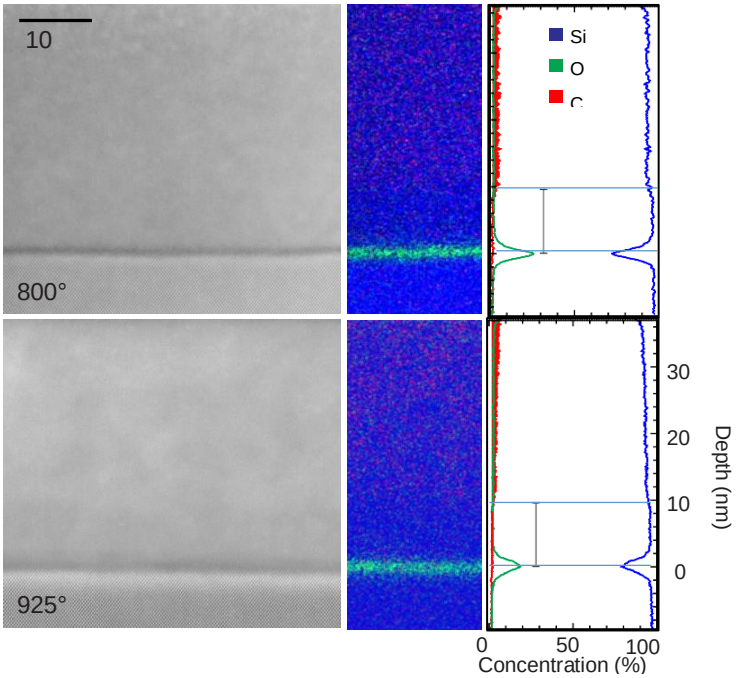

Figure 7: TEM analysis similar to Figure 6, but with a 10 nm thick carbon-free buffer layer w/o doping.

Even when the interfacial layer appears intact in the structural analysis, there may still be changes that compromise the contact structure electrically. Figure 8 shows results of annealing at 800°C for 5 minutes, applied to samples where the buffer layer thickness was varied between 0 and 15 nm. The saturation current density[2] j_0 shows a clear improvement from 37 fA/cm^2 down to 12 fA/cm^2. If the thickness of the buffer layer exceeds 10 nm, passivation is once more lost (j_0 no longer visible on the scale of Figure 8), presumably by insufficient diffusion of boron into the wafer.

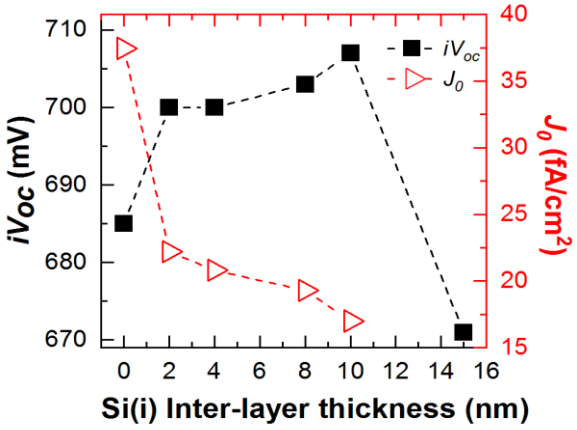

Figure 8: Dependence of j_0 (red) and iVoc (black) on the buffer layer thickness between the interfacial SiOx layer and the p-type SiCx layer; all samples were annealed at 800°C for 5 minutes.

[2] The relation between the saturation current density j_0 and the effective lifetime τ_{eff} is discussed in section 9.2 of the appendix. The measured quantity is still τ_{eff}, but the properties of a given contact structure are better expressed by j_0 because it removes the dependence on the wafer thickness.

After the successful introduction of the buffer layer, further development was carried out by varying the deposition parameters such as doping concentration and carbon content, and different annealing conditions were applied. In all cases the saturation current density was measured to characterize the quality of the passivation, on promising samples also the contact resistivity was measured with the transfer length method (TLM) using a pattern of ITO contacts [19].

The left panel in Figure 9 plots the results for annealing dwell times up to 15 min at temperatures between 800 °C and 900 °C together with projected efficiency contours (c.f. appendix 9.1.3). Compared to the characteristic of the Al-BSF which is reproduced in the lower right corner, the p-type SiCx passivating contacts feature an improvement in saturation current density by ca. two orders of magnitude whereas the contact resistivities are increased by about two orders of magnitude. Nevertheless, the passivating SiCx rear contacts extend over a more favourable part of the efficiency-contours.

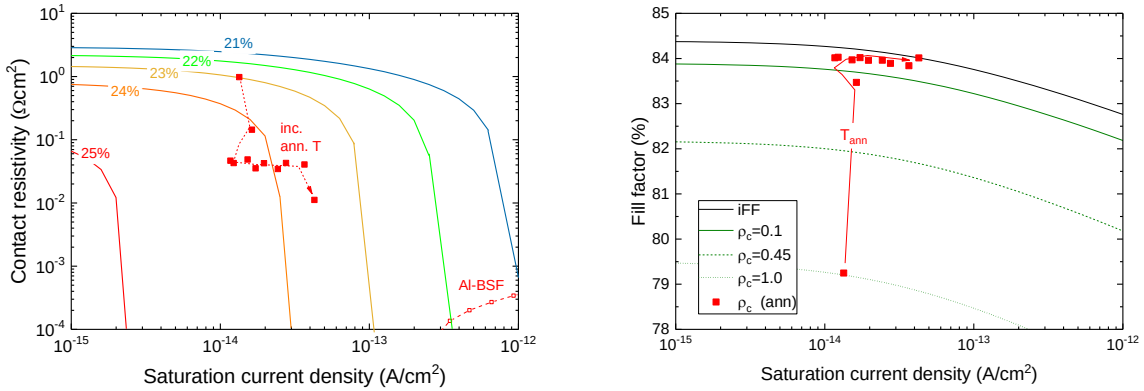

Figure 9: Projected efficiencies (left) and FF values (right) for p-type passivating SiCx contacts based on their measured saturation current densities and their contact resistivities after coating with ITO [19] (full symbols).

Globally it emerges that increasing temperatures or prolonged annealing times reduce the contact resistivity, but at the same time increase the saturation current density. The influence of the contact resistivity is shown more clearly in the right panel of Figure 9. It displays projected values of the FF with the contribution of the contact resistivity as function of the saturation current density (c.f. eq. (3) in appendix 9.2). Most of the investigated samples are not limited by the contact resistivity, the two exceptions are those that were exposed to lowest thermal budgets, i.e. annealing for 1 and 5 min at 800°C. Different from the heterojunctions discussed in section 4.2, p-type passivating SiCx rear contacts have a clear promise to reach FF values between 83 and 84%.

The measurements of the saturation current density and the contact resistivity are powerful tools for the screening of processing conditions. However, the ultimate test for a new contact structure is whether it works in a complete solar cell. To this end, we used the hybrid solar cell structure discussed in Appendix 9.3. The upper left panel in Figure 10 shows that contacts annealed at temperatures below 825°C are capable of delivering Voc up 705 mV, i.e. a large improvement beyond the BSF contact strategy.

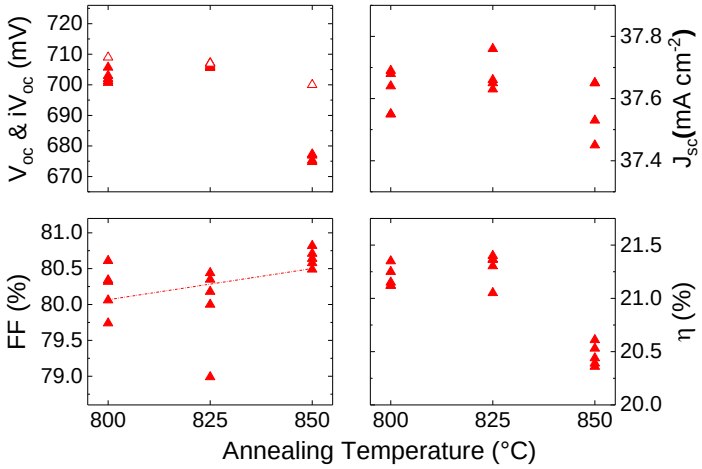

Figure 10: Solar cell parameters of hybrid cells employing annealed p-type SiCx rear contacts and n-type heterojunctions at the front.

Unfortunately, the hybrid design is only of limited use for testing the upper limits of current extraction. Therefore, we developed n-type SiCx passivating contacts for use at the front. The first experiment had to be carried out with flat wafers since the process of the n-type SiCx was not yet compatible with textured surfaces at the time of fabrication. Focussing only on the FF, Figure 11 nevertheless shows a value of 84%. This suggests that annealed passivating SiCx contacts can live up to the full potential expected from Figure 9.

As outlook we cite a last minute result for a textured cell with passivating contacts on both sides.[3] Applying an n-type SiCx contact on the textured front surface of a p-type wafer and co-annealing it with a flat p-type SiCx contact on the rear, a Voc of 717 mV, a FF of 81.3% and a current density of 38.4 mA/cm^2 were obtained; the resulting efficiency is 22.4%. This value improved to 22.6% after application of an MgF_2 double anti-reflection coating.

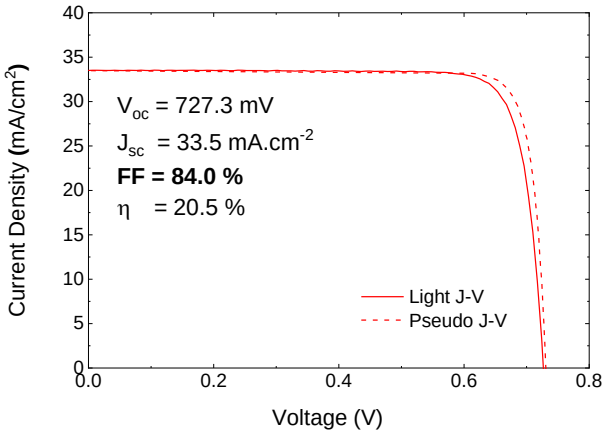

Figure 11: Current-voltage characteristic of a solar cell with annealed SiCx passivating contacts at front and rear. The dashed line represents a pseudo-IV curve which is measured without current flow and thus without series resistance. Note that the current density is lower than Figure 10 because the cell was manufactured on flat wafer without light scattering texture.

[3] Details will be presented by G. Nogay et al. at the upcoming World PVSEC 2018.

4.3.2 Annealed n-type SiOx contacts

The primary motivation to investigate passivating contacts based on SiOx is the use at the front because they are more transparent than SiCx. Similar to the cell design with passivating n-type SiCx front contacts in Figure 11, this is a route towards solar cells with passivating contacts on both sides. The higher transparency of SiOx has the additional benefit of reducing the amount of parasitic absorption.

The n-type SiOx contact was designed as multilayer structure, incorporating the chemical oxide at the interface and a double-layer stack which consists of a nanocrystalline SiOx film and of a nanocrystalline silicon film without oxygen. The SiOx layer within the double-layer stack is phosphorus-doped and deposited from a hydrogen-rich discharge that yields a phase-separation into a crystalline silicon phase and an amorphous matrix. The oxygen-free nanocrystalline film has been added to the stack for two reasons. First, it can protect the underlying oxide against chemical etching processes such an HF dip needed to remove native oxides. Second, oxide films typically expel phosphorous atoms during annealing, resulting in an insufficiently low doping to form a good contact to the ITO layer at the front.

Figure 12 shows that the passivation with n-type SiOx layers generally improves as the annealing temperature is increased to 850°C, and it stays on a high level for annealing temperatures up to 950°C.

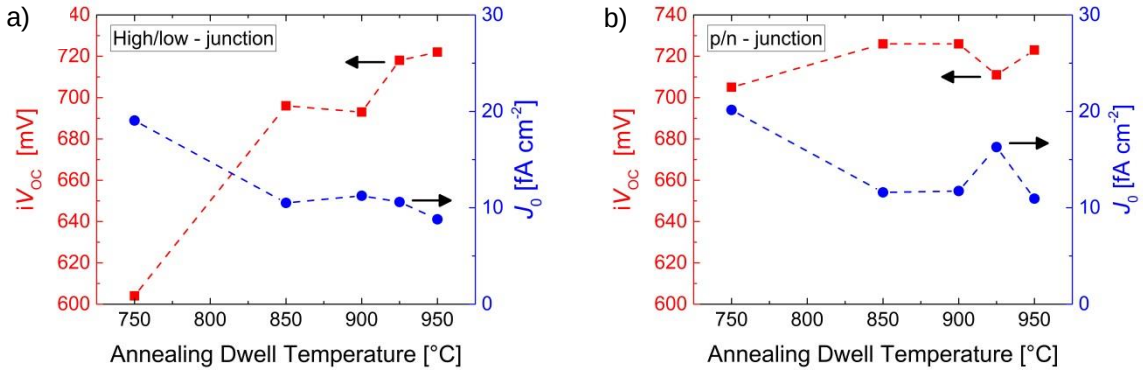

Figure 12: Saturation current (circles) and implied Voc (squares) of passivating n-type contacts on n-type wafers (left panel) and on p-type wafers (right panel).

Different from the SiCx contacts discussed in the previous section, SiOx contacts sustain surprisingly high annealing temperatures without damaging their passivation. Therefore, TEM and elemental mapping was performed similar to the SiCx contacts. Figure 13 shows that the granular structure of the phase-separated oxide film is visible in the as-deposited stack. The chemical mapping reveals that the oxygen content does not change abruptly as expected for a double-layer, but it decreases steadily from the interface towards the front surface. At the same time, the phosphorus content is higher in the part of the stack that was deposited without oxygen.

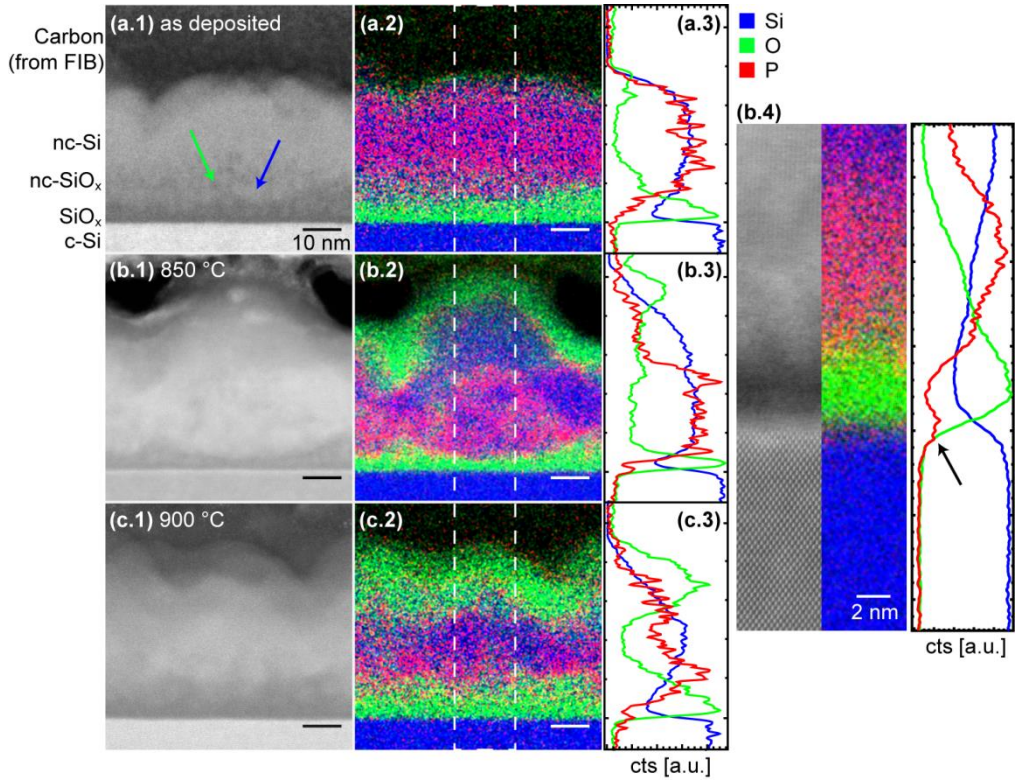

Figure 13: Recrystallization of nanocrystalline SiOx/Si stacks doped with phosphorous. The left panels show cross sections, the middle panels show elemental mappings of the same regions and integrated line scans, the far right shows a high-resolution analysis of the sample annealed at 850°C.

Different from the annealing of the p-type SiCx contact, the interfacial oxide remains intact for annealing at 900°C even without buffer layer. The arrow in the high resolution image on the right side of Figure 13 illustrates that phosphorus is transported through the oxide towards the wafer, but the dopant concentration is visibly reduced within the oxide.

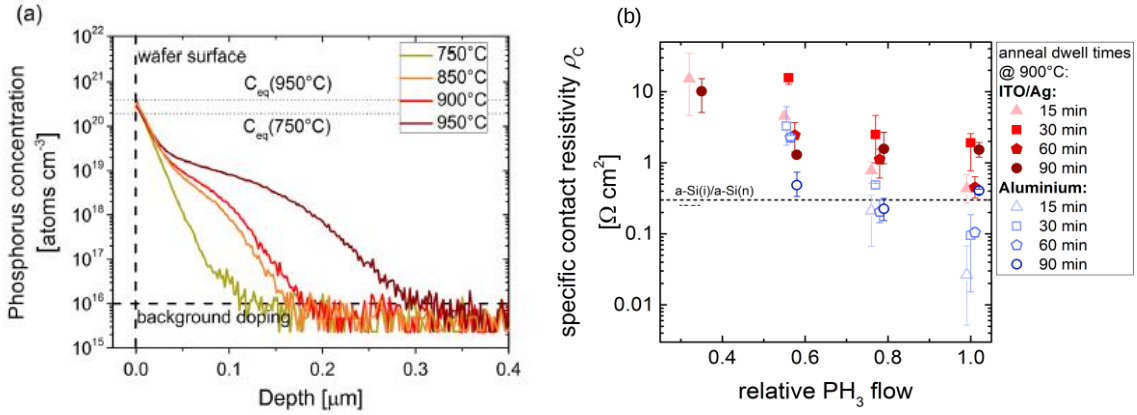

Figure 14: Depth profile of the phosphorous concentration after annealing of n-type SiOx contacts (left) and contact resistivities with ITO (red) and aluminium (blue) [21].

Since the n-type SiOx layers sustain temperatures higher than 900°C, they can serve as efficient source of phosphorous diffusion for the formation of junctions with depth up to 200 nm as shown in Figure 14 a). Figure 14 b) shows the associated contact resistivities with ITO (red symbols) and

aluminium (blue symbols) [21]. The contacts with ITO are relevant for the use at the front, but they are somewhat higher than the ones with aluminium and those of the annealed SiCx contacts quoted in section 4.2. Nevertheless, for high relative PH_3 flow they are still comparable with amorphous n-type contacts of heterojunction solar cells as indicated by the dashed line. According to Figure 9, FF values between 82 and 83% may be expected in solar cells.

An important consideration for junction formation is the stability during subsequent process steps. For heterojunction solar cells using amorphous silicon layers, it was reported that the passivation provided by the intrinsic amorphous layer suffers during ITO sputtering, but recovers almost completely during the subsequent curing step of the ITO and the screen-printed silver metallization [22]. Figure 15 shows the results of a similar experiment with n-type SiOx passivating contacts[21]. In all of the shown cases, the passivation after annealing (red bars) is degraded after ITO sputtering as indicated by the increased saturation current densities (light blue bars). Different from heterojunctions, the curing step recovers the passivation only to a very small extent (dark blue bars).

The two panels of Figure 15 nevertheless show different behaviour for samples deposited with low and high flow ratio of the phosphorous dopant. Before ITO sputtering, samples with lowly doped layers show good passivation (saturation current densities on average between 7 and 10 fA/cm^2), but ITO sputtering degrades them severely as indicated by the light blue bars that reach values between 20 and 33 fA/cm^2. Comparing with the depth profiles of Figure 14 a), lowly doped layers correspond to shallow junctions that are not effective in shielding minority carriers from reaching the interface. Consequently, such samples must rely to a large extent on the quality of the interfacial oxide and whether its defects can be passivated by a hydrogenation step. Figure 14 b) additionally suggests that the contact resistivity of lowly doped layers is too high for current extraction. On the other hand, highly doped layers have slightly worse passivation before ITO sputtering (saturation current densities on average between 10 and 15 fA/cm^2), but they show much less degradation, especially those annealed for 30 and 60 minutes. These conditions yield deeper junctions that shield minority carriers more effectively from reaching the interface, and for the case of long anneals also their contact resistivities are around 0.3 Ωcm^2 which tolerable for FF values above 83%, although it is not yet ideal.

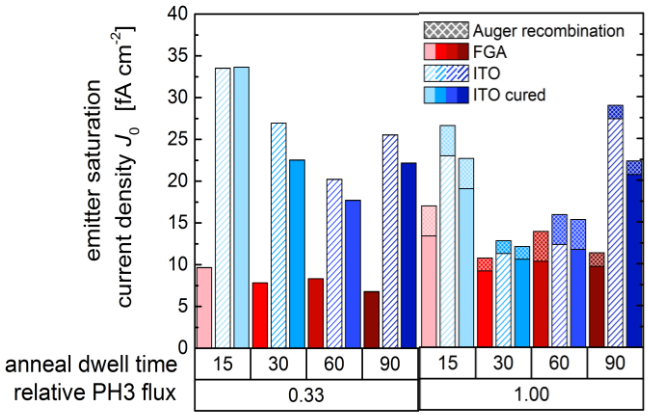

Figure 15: Variation of the saturation current density before ITO sputtering (red), after ITO sputtering (light blue) and after ITO curing (dark blue) for two different dopant flow ratios (0.33 and 1.0) and varying annealing dwell times between 15 and 90 minutes at 900 °C [21].

Conditions close to the optimum of Figure 15 were used for testing a complete solar cell. Also here, the hybrid design discussed in Appendix 9.3 was used, resulting in the characteristic shown in Figure 16. Based on the shown values of the contact resistivity, a FF better than 80% might have been expected, the measured value could therefore be related once more to a limitation of the amorphous

heterojunction. The figure includes a so-called pseudo-iV curve which is a current-voltage characteristic without the influence of the series resistance. It is measured in a Suns-Voc measurement at different light intensities without current-flow. The corresponding characteristic which yields a pseudo-FF of 83%. This result is closer to the values expected on the basis of the contact resistance, confirming that the heterojunction is the limiting factor in the hybrid cell design. Nevertheless, a Voc of 690 mV and an efficiency above 18% demonstrate the potential of this approach.

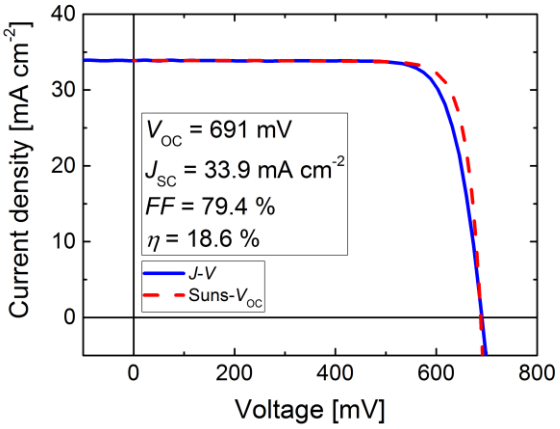

Figure 16: Current-voltage characteristic of a hybrid cell with passivating n-type SiOx contact at the front and a heterojunction at the rear. Note that the cell is flat without light scattering texture. The dashed red line represents a pseudo-IV curve which is measured without current flow and thus without series resistance.

Summarizing the work of WP3, passivating contacts with compatibility to high processing temperatures were developed. Figure 10 shows that p-type SiCx layers tolerate temperatures up to 825°C, which means that they are compatible with the lower end of process temperatures used for the phosphorous-diffusion of n-type front contacts in standard solar cells. An apparent limitation to FF values around 80% is actually a consequence of the chosen type of demonstrator cell. A modified cell process with passivating contacts at the front and at the rear avoids this issue; the FF value of 84% shown in Figure 11 shows that passivating contacts based on SiCx provide excellent current extraction.

4.4 Processing with reduced thermal budget (WP4)

WP4 represents the focus of the third year of this project. Different from the results of the previous sections, work in this WP is devoted to fast annealing processes. This aims at integration with the firing step. Since the heating ramps of firing are typically 50°C/sec, hydrogen is released from the film faster than it can diffuse out, thus its pressure lifts the film from the substrate. This issue called blistering is particularly is pronounced in films with p-type doping because rupture of hydrogen-bonds starts already at 300°C [23]. For firing stable films, either the hydrogen content in the as-deposited films should be low, or hydrogen should be bonded more strongly, such that its release occurs only at higher temperature where diffusion of hydrogen to the surface is more effective.

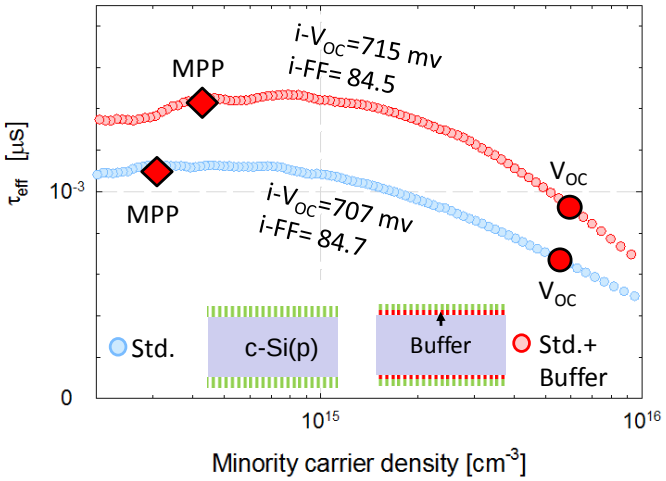

Figure 17: Effective lifetimes (blue, left scale) as function of the minority carrier density of p-type passivating contacts after firing and hydrogenation. Blue curve represent a single layer contact, red curve represent the result incorporating a buffer layer on the interfacial oxide [24].

Figure 17 shows effective lifetimes as function of the injection level for two types of firing-stable contacts. One is a single layer (blue symbols), the other one is a stack of an undoped and of a doped film (red symbols) [24]. At low density of injected minority carriers, both films reach effective lifetimes above 1000 µs, the behaviour at higher injection suggests implied Voc values above 700 mV. Samples with double-layers generally show higher effective lifetimes, indicating better passivation. The associated contact resistivities were found to be below 70 mΩcm^2; the samples with double layer generally had slightly higher value than those with a single layer, but still low enough for a full area passivating contact.

For the development of passivating contacts it is important to know whether the passivation is related to a low density of interface defects or to a doping profile that shields minority carriers from reaching the interface such as shown in Figure 14. To this end, the boron concentration was measured by secondary ion mass spectroscopy (SIMS). Before and after firing, the boron-concentration decays by an order of magnitude over less than 5 nm which is the depth resolution of the SIMS instrument. Consequently, the passivation effect of the fired contacts depends on an efficient hydrogenation of the interface, possibly assisted by a band-bending that is induced from the highly doped layer across the interfacial oxide.

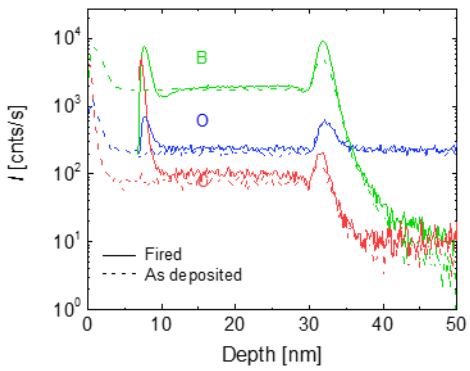

Figure 18: Depth profiles of B and O and C measured by SIMS for before and after firing of the SiC_x(p) .

The novel fired passivating contact was tested in the same type of hybrid cell as the diffused contacts in the previous section. The current-voltage characteristics in Figure 19 show that the cell with the single-layer contact has lower Voc but higher FF than the one with the double layer contact. The behaviour corroborates the results on effective lifetime and contact resistivity shown in Figure 17, even though it is likely that the FF is limited by the heterojunction as it was the case for the annealed SiCx contacts presented in section 4.2.

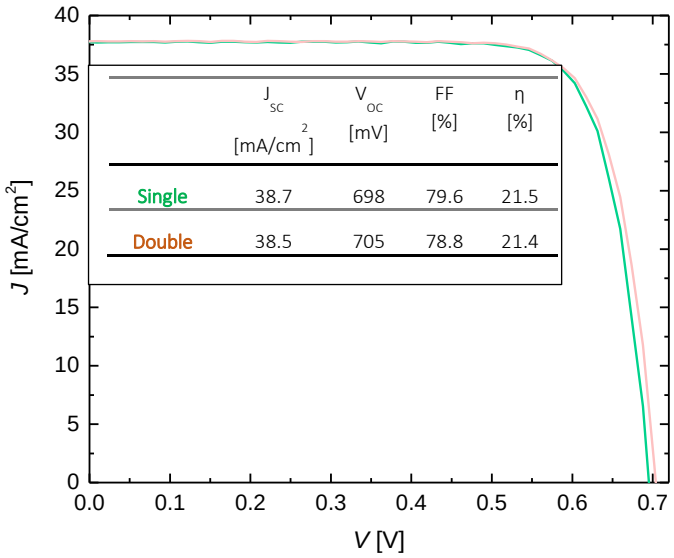

Figure 19: Current voltage characteristics of a hybrid solar cell with fired p-type rear contact. Green and red curves represent single-layer and double-layer contacts, respectively.

Finally, integration into a fully fired device was achieved near the very end of the project in collaboration with CSEM. Therefore, a p-type wafer with $POCl_3$-diffused front contacts and SiNx AR-coating was covered with a fireable p-type passivating SiCx contact at the rear. The front side requires firing under conditions that the metallization-paste sinters through the SiNx anti-reflection coating and contacts the underlying n-type diffused region. The formation of the passivating rear contact had to comply with this process. After firing, the device was finished by sputtering an ITO layer and a silver reflector at the rear. The resulting cell achieved a Voc of 662 mV, a FF of 78.5% and a current density of 41.2 mA/cm^2, resulting in an efficiency of 21.4%.[4] Clearly, the Voc of this cell requires improvement, but the demonstration of a fully operational device shows that fireable passivating rear contacts can be a viable upgrade to the BSF process.

Summarizing the activities of WP4, a passivating p-type SiCx rear contact was successfully developed for firing processes. We found that it works without in-diffused region, an ingredient that was so far assumed to be indispensable for passivating contacts. Nevertheless, the fireable contact provides a high level of passivation as evidenced by Voc values higher than 705 mV in hybrid cells. Based on these results, we were able to show for the first time an integration of a passivating rear contact with the fire-through of a front metallization.

4.5 Cell testing and characterization (WP5 and WP6)

Reliability testing was carried out by exposing different cell types to light soaking under continuous illumination equivalent to one sun, keeping the cell temperature at 30°C. Up to 1000 hours, the heterojunction cell (black symbols) shows a slight improvement which is governed by the passivation

[4] Details of will be presented by A. Ingenito et al. at the upcoming World PVSEC 2018.

and mostly visible through the FF and the Voc. This behaviour was observed on a variety of heterojunction solar cells [25]. Different to the Staebler-Wronski effect in thin film silicon solar, it is a beneficial effect and it is not easily explained by an equilibrium of the defect pool because it its persistent, i.e. it remains after light-soaking and also after annealing.

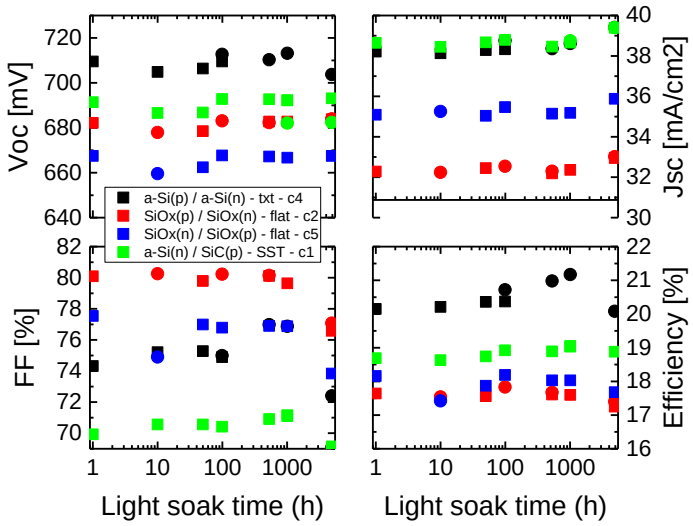

Figure 20: Variation of the solar cell parameters upon light soaking for 5000 hours. Black symbols refer to a heterojunction reference, red and blue symbols refer to a flat cell with co-annealed SiOx passivating contacts on both sides, green symbols refer to a hybrid cell with SiC passivating contact at the rear.

A slight improvement is also observed in the solar cell with the annealed p-type passivating SiCx rear contact (green symbols), but it is possible that the improvement is related to n-type amorphous front contact. In ref. [25] it was reported that p- as well as n-type amorphous contacts show such an improvement. Finally, solar cells with co-annealed passivating SiOx contacts on both sides do not show a clear variation (red and blue symbols).

For light soaking times of more than 1000 hours, it is observed that the FF of all cells deteriorates. This is very likely related to the silver metallization which showed appreciable tarnishing since the cells were not encapsulated against the degradation by ambient air and by humidity.

Summarizing WP5, a variety of characterization tools were applied to the domain on high-temperature passivating contacts as described in the sections on WP3 and WP4. Preliminary tests of reliability in WP6 showed that long time exposure of hybrid cells to UV-illumination has no effects except those expected for the heterojunction present in this type of device.

5 Discussion of results

Over the last three years, the PASSCO project provided a wealth of results on the topic of passivating contacts. Three main axes can be identified:

5.1 Low-temperature passivating contacts

Heterojunction solar cells with passivating layers of amorphous silicon were the subject of WP2, a relatively small work package of this project. We could clearly show that the contact of doped amorphous silicon with ITO suffers from a significant contact resistance which limits the FF to ca. 80%.

Replacement with doped microcrystalline silicon promises to yield lower contact resistivity due to its better doping efficiency. The fill factor could potentially be increased up to ca. 82%, but the work carried out within this project showed that the growth of microcrystalline material requires a minimum thickness beyond its amorphous incubation region. As a result, there is a trade-off between parasitic absorption and gain in FF. A break-through beyond this trade-off will likely require rethinking the contact strategy. Nevertheless, the current status of development found many other applications at the PV-Lab, for example in rear-contacted heterojunction solar cells [31] and as tunnelling junction in perovskite/silicon tandems [32].

5.2 Annealed high-temperature passivating contacts

Annealing is usually associated with slow temperature ramps and long dwell times. In the PASSCO project, we generally tried to employ annealing processes that are compatible with the emitter formation of standard solar cells, i.e. annealing at temperatures between 850 and 900°C and dwell times of minutes or tens of minutes. Section 4.3.1 showed that passivating SiCx contacts resist 850°C for short times whereas SiOx contacts comply even with higher temperatures and longer dwell times. The integration of a passivating rear contact with the phosphorous diffusion of the standard cell process is thus possible, but it would still require a strategy for the metallization.

Reaching out beyond the near future, section 4.3.1 also showed that it is possible to apply passivating SiCx contacts to both sides. The resulting solar cells showed open circuit voltages above 720 mV and excellent fill factors up to 84% on a flat device. The transfer to textured wafers is ongoing, preliminary experiments resulted in cell efficiencies up to 22.6%.

5.3 Fired high-temperature passivating contacts

Fireable passivating contacts were the second high temperature activity in this project and one of high technological relevance. If such contacts could be integrated with the firing step of standard solar cell manufacturing, they could become a true alternative to the BSF contact and thus have an impact on 80% of the photovoltaic market. In the PASSCO project we successfully developed fireable passivating contacts, and we could demonstrate their integration with an industrial firing process, i.e. processing the passivating rear contact at the same time as the front metallization. The resulting device showed a promising efficiency of 21.4%.

6 Conclusions and outlook

In this project, we addressed the challenge to realise passivating contacts for silicon solar cells. Such contacts are needed to achieve high open-circuit voltage, the main limitation of current standard solar cells with metallic full-area rear contact. Since the current financial environment does not favour heavy investment, we took care that our development does not require disruptive changes to the manufacturing process. In essence, our passivating contacts require an interfacial oxide layer, a contact layer of doped silicon, a thermal treatment, and hydrogenation. They apply to the full wafer, there is no need for structuring. We worked primarily with the standard wafer-polarity, i.e. p-type, and the contacts are formed with the thermal budget of existing steps such as the diffusion of the front contact or common firing processes used for metallization formation. The deposition of the doped layer is a key development because it must fulfil a variety of requirements such as single-side processing, excellent adhesion on the underlying oxide, crystallization without damage to the oxide, incorporation of dopants to ensure electric contact, low parasitic absorption, and chemical stability for subsequent

processing steps. We could successfully demonstrate that plasma enhanced chemical vapour deposition can provide multifunctional layers that comply with these requirements.

In the course of the project, we were able to demonstrate compatibility with the thermal treatments commonly used in industrial manufacturing, i.e. long annealing processes at high temperature as well as rapid thermal processing steps. Thus, we can propose passivating contacts that integrate with the phosphorous diffusion used at the very begin of the standard solar cell process, or with the firing of the metallization at the end. We developed hybrid solar cells to test passivation and current extraction of our passivating contacts. The good passivating quality and charge carrier extraction of our fired passivating contact was highlighted by open circuit voltage between 700 and 705 mV and FF in the range of 80%. Recently we have also demonstrated a full integration into an industrial-compatible process. For solar cells employing passivating contacts on both sides, superior passivation quality with open circuit voltages between 720 and 730 mV were demonstrated. Likewise, FF values around 80% and in exceptional cases up to 84% showed that the photocurrent is efficiently extracted by these contacts. Thus, we demonstrated two viable pathways how industries can upgrade their manufacturing lines and remove the bottleneck of the highly recombinative rear metallization.

The project focused on providing contacts with p-type silicon because it still the most widely used wafer material. Nevertheless, n-type wafers were frequently used as witness or as reference. We found that the majority of deposition processes and annealing procedures require only minor adaptations in order to work on n-type wafers. Passivating contacts are thus in an excellent starting position for n-type solar cells in case this material overcomes its current penalty in production cost and gathers a larger share of the photovoltaic market

The project stimulated a fruitful international collaboration, e.g. with the partners of the EU H2020 project “DISC” such as the INES (Chambery), the Fraunhofer ISE (Freiburg), and the ISFH (Hamelin). A more dedicated characterization of passivating contacts will be carried out in a recently started research project with the University of Luxemburg. The key results of the project were protected by filing two patents, one on passivating front contacts with enhanced transparency, and a second on fireable passivating rear contacts; a third filing is being prepared. Transfer to industry was initiated in the framework of a national collaboration with CSEM and Meyer-Burger.

7 Publications

EPFL_2016 G. Nogay, J. P. Seif, Y. Riesen, A. Tomasi, Q. Jeangros, N. Wyrsch, F.-J. Haug, S. De Wolf, and C. Ballif, "Nanocrystalline Silicon Carrier Collectors for Silicon Heterojunction Solar Cells and Impact on Low-Temperature Device Characteristics", IEEE Journal of Photovoltaics 6, p. 1654-1662 (2016).

EPFL_2016 G. Nogay, J. Stuckelberger, P. Wyss, Q. Jeangros, C. Allebé, F. Debrot, X. Niquille, M. Despeisse, F.-J. Haug, P. Löper, and C. Ballif, "Silicon rich silicon carbide hole-selective rear contacts for crystalline silicon based solar cells", ACS Applied Materials & Interfaces 8(51), p. 35660 (2016).

EPFL_2016 J. Stuckelberger, G. Nogay, P. Wyss, Q. Jeangros, C. Allebé, F. Debrot, X. Niquille, M. Ledinsky , Antonin F., Matthieu D., F.-J. Haug, P. Löper , C. Ballif , "Passivating electron contact based on highly crystalline nanostructured silicon oxide layers for silicon solar cells", Solar Energy Materials and Solar Cells, Volume 158, Part 1, December 2016, Pages 2-10

EPFL_2017 J. Stuckelberger, G. Nogay, P. Wyss, A. Ingenito, C. Allebé, J. Horzel, B. A. Kamino, M. Despeisse, F.-J. Haug, P. Löper, and C. Ballif, "Recombination analysis of phosphorus-doped nanostructured silicon oxide passivating electron contacts for silicon solar cells", accepted for publication in IEEE Journal of Photovoltaics (2017).

EPFL_2017 G. Nogay, J. Stuckelberger, P. Wyss, E. Rucavado, C. Allebé, T. Koida, M. Morales-Masis, M. Despeisse, F.-J. Haug, P. Löper, and C. Ballif, "Interplay of annealing temperature and doping in hole selective rear contacts based on silicon-rich silicon-carbide thin films", Solar Energy Materials and Solar Cells 173 (Supplement C), p. 18-24 (2017).

EPFL_2018 I. Mack, J. Stuckelberger, P. Wyss, G. Nogay, Q. Jeangros, J. Horzel, C. Allebé, M. Despeisse, F.-J. Haug, A. Ingenito, P. Löper, C. Ballif, “Properties of mixed phase silicon-oxide-based passivating contacts for silicon solar cells”, Solar Energy Materials and Solar Cells (2018, in press)

EPFL_2018 F. Feldmann, G. Nogay, P. Löper, D.L. Young, B.G. Lee, P. Stradins, M. Hermle, S.W. Glunz, “Charge carrier transport mechanisms of passivating contacts studied by temperature-dependent J-V measurements”, Solar Energy Materials and Solar Cells, Volume 178, May 2018, Pages 15-19

EPFL_2018 A. Ingenito, G. Nogay, Q. Jeangros, E. Rucavado, C. Allebé, S. Eswara, N. Valle, T. Wirtz, J. Horzel, T. Koida, M. Morales Masis, M. Despeisse, F.-J. Haug, P. Löper, C. Ballif, “A Fired Silicon-based Heterojunction (FlaSH) passivating contact for next generation industrial c-Si solar cells”, under review.

8 References

[1] "International Technology Roadmap for Photovoltaics (ITRPV)."

[2] A. W. Blakers, A. Wang, A. M. Milne, J. Zhao, and M. A. Green, "22.8% efficient silicon solar cell," *Appl. Phys. Lett.*, vol. 55, no. 13, pp. 1363–1365, 1989.

[3] T. Lauermann, B. Fröhlich, G. Hahn, and B. Terheiden, "Diffusion-based model of local Al back surface field formation for industrial passivated emitter and rear cell solar cells," *Prog. Photovoltaics Res. Appl.*, vol. 23, no. 1, pp. 10–18, 2015.

[4] T. Dullweber *et al.*, "PERC+: Industrial PERC solar cells with rear Al grid enabling bifaciality and reduced Al paste consumption," *Prog. Photovoltaics Res. Appl.*, vol. 24, no. 12, pp. 1487–1498, 2016.

[5] J.-Y. Gan and R. M. Swanson, "Polysilicon emitters for silicon concentrator solar cells," in *Photovoltaic Specialists Conference, 1990., Conference Record of the Twenty First IEEE*, 1990, pp. 245–250.

[6] A. Richter, J. Benick, F. Feldmann, A. Fell, M. Hermle, and S. W. Glunz, "n-Type Si solar cells with passivating electron contact: Identifying sources for efficiency limitations by wafer thickness and resistivity variation," *Sol. Energy Mater. Sol. Cells*, vol. 173, pp. 96–105, 2017.

[7] F. Feldmann, M. Bivour, C. Reichel, H. Steinkemper, M. Hermle, and S. W. Glunz, "Tunnel oxide passivated contacts as an alternative to partial rear contacts," *Sol. Energy Mater. Sol. Cells*, vol. 131, pp. 46–50, 2014.

[8] F. Feldmann, M. Simon, M. Bivour, C. Reichel, M. Hermle, and S. W. Glunz, "Efficient carrier-selective p-and n-contacts for Si solar cells," *Sol. energy Mater. Sol. cells*, vol. 131, pp. 100–104, 2014.

[9] F. Feldmann, M. Simon, M. Bivour, C. Reichel, M. Hermle, and S. W. Glunz, "Carrier-selective contacts for Si solar cells," *Appl. Phys. Lett.*, vol. 104, no. 18, p. 181105, 2014.

[10] F. Feldmann, M. Bivour, C. Reichel, M. Hermle, and S. W. Glunz, "Passivated rear contacts for high-efficiency n-type Si solar cells providing high interface passivation quality and excellent transport characteristics," *Sol. Energy Mater. Sol. Cells*, vol. 120, pp. 270–274, 2014.

[11] M. J. Kerr and A. Cuevas, "General parameterization of Auger recombination in crystalline silicon," *J. Appl. Phys.*, vol. 91, no. 4, pp. 2473–2480, 2002.

[12] H. Kobayashi Asuha, O. Maida, M. Takahashi, and H. Iwasa, "Nitric acid oxidation of Si to form ultrathin silicon dioxide layers with a low leakage current density," *J. Appl. Phys.*, vol. 94, no. 11, pp. 7328–7335, 2003.

[13] K. M. Gad *et al.*, "Improved Si/SiOx interface passivation by ultra-thin tunneling oxide layers prepared by rapid thermal oxidation," *Appl. Surf. Sci.*, vol. 353, pp. 1269–1276, 2015.

[14] A. Moldovan, F. Feldmann, M. Zimmer, J. Rentsch, J. Benick, and M. Hermle, "Tunnel oxide passivated carrier-selective contacts based on ultra-thin SiO2 layers," *Sol. Energy Mater. Sol. Cells*, vol. 142, pp. 123–127, 2015.

[15] G. Nogay *et al.*, "Nanocrystalline Silicon Carrier Collectors for Silicon Heterojunction Solar Cells and Impact on Low-Temperature Device Characteristics," *IEEE J. Photovoltaics*, vol. 6, no. 6, 2016.

[16] M. A. Green, “Accuracy of analytical expressions for solar cell fill factors,” *Sol. Cells*, vol. 7, no. 3, pp. 337–340, 1982.

[17] F. Sahli *et al.*, “Improved optics in monolithic perovskite/silicon tandem solar cells with a nanocrystalline silicon recombination junction,” *Adv. Energy Mater.*, vol. 8, no. 6, 2018.

[18] A. Tomasi *et al.*, “Simple processing of back-contacted silicon heterojunction solar cells using selective-area crystalline growth,” *Nat. Energy*, vol. 2, no. 5, p. 17062, 2017.

[19] G. Nogay *et al.*, “Interplay of annealing temperature and doping in hole selective rear contacts based on silicon-rich silicon-carbide thin films,” *Sol. Energy Mater. Sol. Cells*, vol. 173, 2017.

[20] G. Nogay *et al.*, “Silicon-Rich Silicon Carbide Hole-Selective Rear Contacts for Crystalline-Silicon-Based Solar Cells,” *ACS Appl. Mater. Interfaces*, vol. 8, no. 51, 2016.

[21] J. Stuckelberger *et al.*, “Recombination Analysis of Phosphorus-Doped Nanostructured Silicon Oxide Passivating Electron Contacts for Silicon Solar Cells,” *IEEE J. Photovoltaics*, vol. 8, no. 2, 2018.

[22] B. Demaurex, S. De Wolf, A. Descoeudres, Z. Charles Holman, and C. Ballif, “Damage at hydrogenated amorphous/crystalline silicon interfaces by indium tin oxide overlayer sputtering,” *Appl. Phys. Lett.*, vol. 101, no. 17, p. 171604, 2012.

[23] S. De Wolf and M. Kondo, “Boron-doped a-Si: H/c-Si interface passivation: Degradation mechanism,” *Appl. Phys. Lett.*, vol. 91, no. 11, p. 112109, 2007.

[24] and C. B. A. Ingenito, G. Nogay, Q. Jeangros, M. E., C. Allebé, J. Horzel, M. Despeisse, F.-J. Haug, P. Löper, “A novel fired silicon-based heterojunction for high efficiency industrial c-Si solar cells,” in *27th PVSEC Shiga*, 2017.

[25] E. Kobayashi *et al.*, “Increasing the efficiency of silicon heterojunction solar cells and modules by light soaking,” *Sol. Energy Mater. Sol. Cells*, vol. 173, 2017.

[26] E. Yablonovitch, D. L. Allara, C. C. Chang, T. Gmitter, and T. B. Bright, “Unusually low surface-recombination velocity on silicon and germanium surfaces,” *Phys. Rev. Lett.*, vol. 57, no. 2, p. 249, 1986.

[27] S. W. Glunz, A. B. Sproul, W. Warta, and W. Wettling, “Injection-level-dependent recombination velocities at the Si-SiO2 interface for various dopant concentrations,” *J. Appl. Phys.*, vol. 75, no. 3, pp. 1611–1615, 1994.

[28] A. Richter, S. W. Glunz, F. Werner, J. Schmidt, and A. Cuevas, “Improved quantitative description of Auger recombination in crystalline silicon,” *Phys. Rev. B*, vol. 86, no. 16, p. 165202, 2012.

[29] R. Hezel and R. Schörner, “Plasma Si nitride—A promising dielectric to achieve high-quality silicon MIS/IL solar cells,” *J. Appl. Phys.*, vol. 52, no. 4, pp. 3076–3079, 1981.

[30] H. Morita, A. Sato, H. Washida, T. Kato, and A. Onoe, “Efficiency improvement of solar cell utilizing plasma-deposited silicon nitride,” *Jpn. J. Appl. Phys.*, vol. 21, no. S2, p. 47, 1982.

[31] M. Rüdiger, J. Greulich, A. Richter, and M. Hermle, “Parameterization of free carrier absorption in highly doped silicon for solar cells,” *IEEE Trans. Electron Devices*, vol. 60, no. 7, pp. 2156–2163, 2013.

[32] H. H. Berger, “Contact resistance and contact resistivity,” *J. Electrochem. Soc.*, vol. 119, no. 4, pp. 507–514, 1972.

[33] A. M. Cowley and S. M. Sze, “Surface states and barrier height of metal-semiconductor systems,” *J. Appl. Phys.*, vol. 36, no. 10, pp. 3212–3220, 1965.

[34] F. A. Padovani and R. Stratton, “Field and thermionic-field emission in Schottky barriers,” *Solid. State. Electron.*, vol. 9, no. 7, pp. 695–707, 1966.

[35] A. Y. C. Yu, “Electron tunneling and contact resistance of metal-silicon contact barriers,” *Solid. State. Electron.*, vol. 13, no. 2, pp. 239–247, 1970.

[36] D. L. Young *et al.*, “Carrier selective, passivated contacts for high efficiency silicon solar cells based on transparent conducting oxides,” *Energy Procedia*, vol. 55, pp. 733–740, 2014.

[37] J. Zhao, A. Wang, and M. A. Green, “24.5% Efficiency silicon PERT cells on MCZ substrates and 24.7% efficiency PERL cells on FZ substrates,” *Prog. Photovoltaics Res. Appl.*, vol. 7, no. 6, pp. 471–474, 1999.

[38] M. Taguchi *et al.*, “24.7% record efficiency HIT solar cell on thin silicon wafer,” *IEEE J. Photovoltaics*, vol. 4, no. 1, pp. 96–99, 2014.

[39] K. Masuko *et al.*, “Achievement of more than 25% conversion efficiency with crystalline silicon heterojunction solar cell,” *IEEE J. Photovoltaics*, vol. 4, no. 6, pp. 1433–1435, 2014.

[40] D. E. Kane and R. M. Swanson, “Measurement of the emitter saturation current by a contactless photoconductivity decay method,” in *IEEE photovoltaic specialists conference. 18*, 1985, pp. 578–583.

9 Appendix

9.1 Appendix 1: Passivation and contact resistivity

Passivating contacts should provide surface passivation and electrical conductivity in one single entity. This is not evident since common passivating materials – silicon-oxide, silicon nitride, and aluminium oxide – are excellent insulators whereas typical contact materials – metals – result in highly recombinative interfaces.

9.1.1 Passivation

The free surface of covalent semiconductors such as silicon or germanium is characterized by unpaired bonding orbitals that are filled by a single electron. These are called dangling bonds and they can easily capture a second electron from a filled state of the conduction band. They can just as easily lose their unpaired electron by capturing a hole from the valence band. In a solar cell, electron-hole pairs are generated by the absorption of light, and can easily get lost by recombination at a dangling bond state of the surface. In case of silicon, the energy of the dangling bonds is located close to the middle of the bandgap, making them particularly strong recombination centres.

The recombination at dangling bond states can be suppressed by two methods. The first is called **chemical passivation** and works by saturating the dangling bonds with a suitable bonding partner that removes the energetic state of the bond from the bandgap. The simplest method to achieve this goal is chemical passivation with a monolayer of hydrogen [26]. Alternatively, the surface can be oxidized to form silicon oxide which is an inert material that bonds to silicon with a low density of interface defects [27]. The second passivation method is called **field effect passivation** and works by repelling one type of charge carrier from the interface. For example, Al_2O_3 provides field effect passivation to p-type silicon because it contains a high density of negative charge that repels the minority carriers – electrons - away from the interface [28]. The interface states between silicon and Al_2O_3 may still be defective and capture holes, but these can no longer recombine because there are no electrons available. Likewise, Si_3N_4 is used to passivate the surface of the n-type emitter at the front of silicon solar cells because it contains a positive charge that repels minority carriers, in this case holes [29, 30]. [31]

As the name “back surface field” suggests, the idea of repelling minority carriers away from the interface is also used in the BSF design shown in Figure 1. However, the repulsion does not work by negative charge in a layer outside of the wafer, but by a highly doped region within the wafer. In order to repel electrons, doping must be p-type. The process of solar cells with BSF can be made very lean because p-type doping and the formation of the rear contact are achieved together with the formation of the front contact in a single step during the firing at the end of the fabrication process. As soon as the firing temperature exceeds 660°C, the screen-printed aluminium-paste at the rear melts and mixes with silicon to form an eutectic liquid. Upon cooling, silicon solidifies by incorporating the saturation concentration of aluminium. This yields a heavily aluminium-doped p-type region at the rear of the wafer and upon further cooling a mixed layer of aluminium and silicon that forms the metallic rear contact.

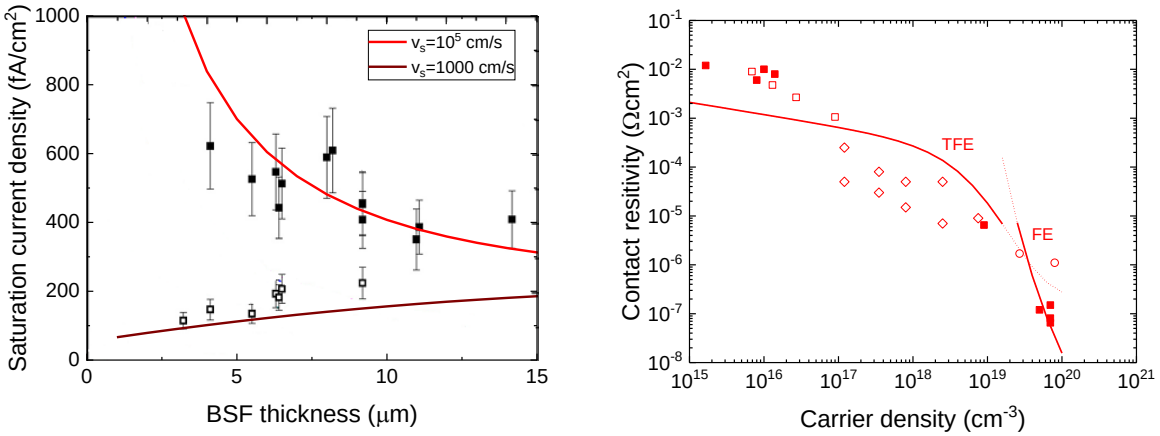

Figure 21: The left panel shows the saturation current density vs thickness of the Al-BSF, data from [31]; the lines illustrate constant Al-doping of 3x10^{18} cm^{-3} and surface recombination velocities v_s of 1'000 and 100'000 cm/s, respectively. The right panel shows the variation of the contact resistivity vs. doping concentration for junctions of p-type crystalline silicon and aluminium, data from [32]. Lines illustrate tunnelling (field emission, FE) and thermally assisted tunnelling (TFE).

The quality of surface passivation is generally assessed by measuring the effective lifetime τ_{eff} of the minority carriers which yields the saturation current density $j_{0,surf}$ (c.f. section 9.2). Essentially $j_{0,surf}$ is a measure of the charge carrier flow that is lost due to recombination at an interface, i.e. the lower its value, the better is the passivation. The left panel in Figure 21 shows values of $j_{0,surf}$ for typical thicknesses of the Al-BSF [31]. Solid symbols represent the highly recombinative interface with aluminium; open symbols represent a measurement after the removal of aluminium and covering with a passivating film of Al_2O_3. Superimposed is a very simple analytical approximation, assuming a constant aluminium doping concentration throughout the thickness of the BSF region. A value of 3x10^{18} cm^{-3} was used, equal to the solubility limit of aluminium in silicon at the solidification temperature of the eutectic which is 577°C. The simple analytic model can be used to estimate values for the surface recombination velocity which are 100'000 cm/s for the interface with aluminium (closed symbols) and 1000 cm/s for the interface passivated with Al_2O_3 (open symbols).

9.1.2 Contact resistivity

The contact between semiconductors and metals can be described as Schottky-junction, but the description requires corrections for the effective transport barrier [33] and for the influence of tunnelling in case of high doping concentrations in the semiconductor [34, 35]. The right panel in Figure 21 collects published values of the contact resistivity ρ_c between crystalline silicon and aluminium [32]. Superimposed are the characteristics for thermionic field emission (TFE) at low carrier concentration and the one for tunnelling (field emission, FE), using an effective barrier height of 0.4 eV.

9.1.3 Projected efficiency limit

The efficiency of a solar cell is the product of the short circuit current density j_{sc}, the open circuit voltage V_{oc} and the fill factor FF. The j_{sc} is mostly governed by the optics of the cell design, but the two others are related to the properties of the contact because the saturation current density j_0 governs the obtainable V_{oc} and the contact resistivity ρ_c reduces the FF as described in section 9.2. If j_0 and ρ_c are known, it is possible to project an upper limit for efficiency that a solar cell with this contact may achieve. This yields the efficiency contours shown in Figure 22.

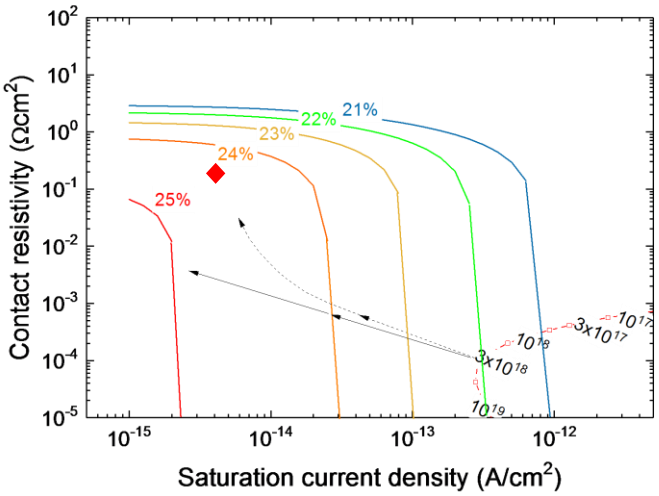

Figure 22: Contours of upper efficiency limits related to the saturation current and the resistivity of the contact (full lines). Open squares illustrate the properties of an Al-BSF rear contact with thickness of 8 µm and various doping concentrations and according to Figure 21. The arrows illustrate the effect of reducing the contact area to 10% or 1%. The red diamond illustrates the properties estimated for heterojunction devices [36].

Figure 22 includes the characteristic expected for an aluminium rear-contact according to the data collected in Figure 21 It underlines that this contact provides excellent contact resistivity, but that it is limited by recombination as evidenced by its high saturation current densities. Figure 22 also shows a fortuitous coincidence because the saturation-concentration of aluminium in silicon is ca. 1 to 3x10^{18} cm^{-3} at the temperatures used for firing, i.e. close to the optimum of the characteristic.

Figure 22 illustrates the effect of reduced contact area in a PERC design. The arrows represent the effect of reducing the contact area at the rear. For example, a reduction to 10% will increase the area-averaged contact resistivity by a factor of 10 since Al_2O_3 is insulating. If the passivation were perfect, it would reduce j_0 by a factor of 10. As a result, the limiting efficiency could be taken from 22% on the green contour to 24% on the orange contour. However, Figure 21 shows that the saturation current density of a passivation with Al_2O_3 cannot be assumed as zero, thus the area-averaged saturation current density will reduce to a lesser degree as indicated by the dashed arrow. A further reduction of the contact area to 1% would suggest a potential efficiency close to 25% in an idealized scenario, but in this case additional effects of current crowding into the small contact areas will increase the area-averaged contact resistance as indicated by the dashed arrow that curves upwards.

The concept of localized contacts in the PERC design was further improved by minimizing Auger recombination, a recombination effect associated with the high doping concentrations that are needed for low contact resistivity with the metallization. The improvement was achieved by restricting the doping at the rear of the wafer to the small areas underneath the contacts, resulting in the **P**assivated **E**mitter and **R**ear **L**ocally diffused cell (PERL) which reached an efficiency of 25% in 1999 [37]. However, localizing the diffusion and aligning it with the contact areas makes the process rather complicated. Ultimately, the concept of localized contact areas still limits the cell efficiency by recombination at the contact to the metal as evidenced by the Voc of 706 mV in the PERL cell. This limitation prevented any further improvements with this cell concept.

Following a radically different approach, Panasonic routinely achieved Voc values higher than 740 mV with full-area passivating contacts and finally demonstrated an efficiency of 24.7% in 2014 [38]. Shortly thereafter, they demonstrated a certified a world record efficiency of 25.6% by putting both contact polarities on the rear side [39].

9.2 Appendix 2: Relation between lifetime and implied efficiency

The lifetime is a parameter of overarching importance because it is accessible contact-free and non-destructive through a measurement of the photo-conductance. It is measurable already on the bare wafer and it remains measurable throughout almost all of the subsequent processing steps. It is normally called “effective lifetime” because it contains contributions from recombination at defect states in the bulk and at the surface. Focussing on these two effects and neglecting additional limitations due to the Auger effect and radiative recombination which are relevant for very high injection, the effective lifetime of a symmetric sample can be expressed as follows (eq. 11 in [28]):

$$\frac{1}{\tau_{eff}} = \frac{1}{\tau_{bulk}} + 2 \cdot \frac{v_s}{W} \quad \textbf{(1)}$$

Here, W is the wafer thickness and v_s is the surface recombination velocity. Symmetric means that both sides of the wafer are covered with the same structure. Whereas such samples would not occur in the final cell process, they are very valuable for characterization. The surface recombination velocity can be distinguished from bulk recombination because it depends on the injection level Δn (eqns. 9 and 10 in [40]):

$$v_s = \frac{j_0 \Delta n}{q n_i^2} \quad \textbf{(2)}$$

Here, q and n_i^2 are the elementary charge and the intrinsic carrier density, respectively. The formula defines the saturation current density j_0 which is a fundamental parameter to describe the recombination properties of the surface or a contact structure. A saturation current density can also be defined for recombination effects in the bulk of the wafer.

Once j_0 is known, the implied open circuit voltage ($iVoc$) can be estimated with two simple assumptions for the diode quality factor n (e.g. a value of 1.1) and for the short circuit current density j_{sc} of the final device (e.g. 40 mA/cm^2).

$$iV_{oc} = \frac{nkT}{q} \cdot \ln\left\{\frac{j_{sc}}{j_0}\right\} \quad \textbf{(3)}$$

Note that the saturation current densities are additive quantities when they have the same exponential relationship between current and voltage, we can express j_0 as $j_0 = j_{0,surf} + j_{0,bulk}$. In eq (3), k and T are the Boltzmann constant and the absolute temperature, respectively. An upper limit for the fill factor without influence of the series resistance (FF_0) can then be calculated (eq. 2 in [16]):

$$FF_0 = \frac{\frac{qV_{oc}}{nkT} + 1}{1.015 \cdot \frac{qV_{oc}}{nkT} + 5.7} \quad \textbf{(4)}$$

Whereas j_0 describes recombination in very general terms even without contact, the contact resistivity ρ_c requires the connection to an external circuit, ideally for a measurement with the transfer length method (TLM). The contact resistivity acts as series resistivity R_s that will reduce FF_0 to a more realistic value FF_s (Table 1 in [16]):

$$FF_s = FF_0\left(1 - \frac{R_s \cdot j_{sc}}{V_{oc}}\right) + \frac{\left(\frac{R_s \cdot j_{sc}}{V_{oc}}\right)^2}{5.4} \quad \textbf{(5)}$$

Finally the projection of an upper limit of the efficiency is obtained by multiplying all three parameters:

$$\eta = Voc \cdot j_{sc} \cdot FF_s \quad \textbf{(6)}$$

Figure 22 plots contour lines of projected efficiencies between 20 and 25%. Once j_0 and ρ_c of a contact structure are measured, its location on the graph can tell immediately whether a contact strategy will be limited by recombination or resistance and, more importantly for development, where improvements should aim at.

9.3 Appendix 3: Test cell configurations

In case of the p-type SiCx rear contacts, an adequate integration into complete cells would be in combination with a phosphorous-diffused front junction. Unfortunately the needed infrastructure was not available at PV-Lab throughout most of the PASSCO project. In order to provide at least a minimum working environment, we developed a hybrid cell design. Note that this type of device serves purely as tool for characterizing the photo-voltage under illumination and the extraction of current, but it is not intended for industrialization.

The hybrid design was chosen for several reasons:

- Heterojunctions provide excellent surface passivation as shown by Voc values up to 720 mV in Figure 5. This means that whenever a lower Voc value is measured in a hybrid cell, it represents the passivation quality of the tested rear contact.
- Heterojunctions are processed in a temperature range where high-temperature passivating contact are fully stable.
- Heterojunctions were available at PV-Lab (c.f section 4.2 on WP2).

The process flow for a hybrid cell with p-type passivating SiCx contact was as follows: The passivation quality of high-temperature passivating contacts was developed by studying symmetric lifetime samples. On selected ones the contact resistivity was characterized. Finally, the optimum conditions were applied to one side of a cleaned wafer,[5] including anneal and hydrogenation. Subsequently, the other side was texture-etched and covered with an n-type heterojunction. Finally solar cells were completed by adding ITO layers on both sides, followed by full area sputtering of the rear metallization and screen printing of a contact grid at the front, resulting in the pattern of five cells that is shown on the title page.

Only minor changes are needed to manufacture hybrid cells with n-type passivating front contact.

It emerged that the hybrid cells have a big drawback: Figure 5 and Figure 9 suggest that the contact resistivities in amorphous heterojunctions limit the obtainable FF values to ca. 82% whereas the contact resistivities of high-temperature passivating contacts are compatible with higher values. Figure 10 reveals that the hybrid cell is not a very good test structure to assess the properties of current extraction. This difficulty could only be resolved by using high-temperature passivating contacts on both sides, but it required the complete development of an n-type SiCx contact that is compatible with the annealing conditions of the rear contact.

[5] Note that this is a unique strength of the PE-CVD process. A more commonly used deposition method in solar cell manufacturing is LP-CVD, but it apples usually to both sides.